Structural investigation of shear performance of square CFST column joints with extended hollo-bolts

Partha Pratim Debnath[1] and Tak-Ming Chan, M. ASCE[2*]

[1] Postdoctoral Fellow, Department of Civil and Environmental Engineering,
The Hong Kong Polytechnic University, Hung Hom, Kowloon, Hong Kong
E-mail: partha-p.debnath@polyu.edu.hk

[2] Professor, Department of Civil and Environmental Engineering,
The Hong Kong Polytechnic University, Hung Hom, Kowloon, Hong Kong
*Corresponding e-mail: tak-ming.chan@polyu.edu.hk

Abstract

The performance of concrete-filled steel tubular (CFST) column joints with a group of extended hollo-bolts have been experimentally investigated under the influence of shear loading. The primary focus was to understand the performance of extended hollo-bolts in enhancing the transfer of shear load to the concrete core of the column by bolt bearing. The joint assembly was fabricated with rigid end-plate, thereby overcoming the influence of endplates in the joint global behaviour. A series of full-scale group hollo-bolted CFST column joint tests were carried out, where eight specimens were fabricated with group of two hollo-bolts, arranged in one row and two rows in the assembly; another five specimens were fabricated with group of four hollo-bolts, arranged in two rows. Apart from bolt arrangement, the other parameters studied include, use of standard and extended hollo-bolt, embedment length of hollo-bolt, and bolt pitch distance. From the investigation it is observed that, all the joints failed in pure shear signifying utilisation of full capacity of the hollo-bolt, and no prominent bearing failure of concrete was observed. Enhanced composite behaviour was achieved using the extended hollo-bolts as the shear load was transferred to the concrete core effectively. Group of two extended hollo-bolts in single row transmits equal forces to the concrete core, whereas, when two or four extended hollo-bolts are in two rows, the upper row transmits more forces as compared to the bolts in the lower row. Lastly, with pitch

distance of 2.5 times bolt hole diameter and beyond, the total strength of the joint is equal to sum of strength of individual bolts, which confirms that the group action did not deteriorate the joint capacity. Subsequently, an analytical model for the global force-displacement behavior and joint shear strength is proposed by calibrating the test data obtained through this study.

Keywords: Concrete-filled steel tubular (CFST) column, Composite behavior, Blind-bolts, Joints, Shear loading

Introduction

Tubular structures that are usually used in three-dimensional systems, are popular in the construction industry due to its superior structural efficiency and aesthetic appeal. Apart from hollow steel tubes, the concrete filled steel tubes (CFST) have also widely been used as the infill concrete delays the local buckling of the outer tube thereby utilising the strength of steel, and in turn, the tube provides confinement to concrete, thereby enhancing the concrete strength and ductility (Abramski, 2018, Chen et al., 2021). Moreover, in recent years, apart from the conventional square, rectangular and circular CFSTs, polygonal shaped concrete-filled tubes have also been studied to a considerable extent (Zhu and Chan, 2018a, Zhu and Chan, 2018b, Fang et al., 2021). Commonly, the welding technology is adopted for the fabrication of the moment-resisting joints between the steel beam and hollow or CFST column members, but the fabrication can be cumbersome (Jiang et al., 2018) as it creates heat affected zones in the joints leading to stress concentration and also requires skilled works, and thus expensive. On the other hand, the fabrication of bolted joints between an open-steel section member, and hollow or CFST column has been popular due to faster and easier construction, and requires only semi-skilled workers. For the fabrication of bolted joints, the blind-bolts are usually used, as they can be tightened without accessing the inside of the hollow steel tube member. Different type of blind-bolts used in industry and being developed by researchers include, the Ajax blind-bolt (AJAX, 2002), Lindapter hollo-bolt (Lindapter, 2018), T-head one-side blind-bolt (Wang et al., 2021b), the slip-critical blind-bolt (Wang et al., 2017), and the thread-fixed one-side bolts (Wang et al., 2020). Research studies with hollo-bolts, T-shaped and thread-fixed one-side blind-bolts have been conducted for evaluating their performance for joints with hollow steel tubes (Wang et al., 2009, Sun et al., 2020, Wang et al., 2021a, Liu et al., 2021). Experimental investigations for different blind-bolted joints with CFST columns under various loading scenarios have been conducted, and observed reliable performance (Thai et al., 2017, Jiao et al., 2020, Sun et al., 2021, Gao et al., 2022). But developing a moment-resisting bolted joint has always been a challenge for structural engineers. As reported by researchers, in blind-bolted steel tubular joints, the blind-bolt fasteners does not have sufficient stiffness, and under moment loading, severe column wall deformation and slippage of bolts were observed (Tizani and Pitrakkos, 2015, Jeddi and Sulong, 2018), indicating that with the standard blind-bolt only nominally pinned joints can be developed.

To address the above issue and fully exploit the advantages of CFST column and the blind-bolting technology to develop moment-resisting frames, researchers have proposed several modifications of blind-bolts to enhance the joint performance. The blind-bolts were extended by welding the shank with straight and cogged bars and embedding it in the concrete core of the CFST column and observed improved strength and stiffness (Goldsworthy and Gardner, 2006, Yao et al., 2008), but due to the weld between the blind-bolt and cogged extension, brittle failure was also reported. Later, headed anchored blind-bolt was proposed (Agheshlui et al., 2016a, Agheshlui et al., 2016b), where the shank with headed nut provides anchorage to the concrete in CFST column, and pull-out tests were conducted which shows higher performance as compared to standard blind-bolts. The Ajax blind-bolt was also modified to double-headed anchored blind-bolt, and its individual and group performance with circular and square CFST columns was assessed, and enhanced stiffness with delayed crack formation was observed (Oktavianus et al., 2017a, Oktavianus et al., 2017b, Pokharel et al., 2021). Experimental investigation of demountable CFST K-joints with anchored Ajax blind-bolt has also been recently conducted (Yu et al., 2023). Similarly, the Lindapter hollo-bolt (Lindapter, 2018) was modified by elongation of the internal bolt shank with headed nut, and the pull-out test results provides better performance due to the mechanical anchorage (Pitrakkos and Tizani, 2013). The fatigue performance of the extended hollo-bolt was also observed to be similar to standard bolt and nut system (Tizani et al., 2014). The standard and the extended hollo-bolt are shown in Figure 1(a). A schematic diagram of the hollo-bolted beam to CFST column joint is presented in Figure 1(b), and the cross-section of the joint with standard and extended hollo-bolt is shown in Figure 1(c). The anchored blind-bolt protrusion in to the concrete core can also overcome the issues of tube-concrete bond strength based on which the load introduction occurs in the CFST column, as the bond strength tends to decrease with increase in CFST column dimension (Debnath et al., 2023).

Investigation on anchored or extended hollo-bolted CFST column to beam joint under cyclic loading was conducted by Tizani et al. (Tizani et al., 2013a, Tizani et al., 2013b) which mostly had bolt fracture, and observed that the strength, stiffness degradation, rotation capacity and energy dissipation was improved as compared to the standard hollo-bolted joints, but in the study the influence of endplate was not incorporated. Further investigation of failure modes of extended hollo-bolted CFST joints under tensile loading were carried out by experimental, numerical and analytical studies (Tizani et al., 2020, Cabrera et al., 2020, Debnath and Chan, 2021a, Debnath and Chan, 2021b, Debnath and Chan, 2022a), and reported the combined failure modes. Only a limited number of tests can be found in the literature that investigates the shear performance of hollo-bolted CFST column joints. Hollo-bolted angle and channel joints with tubular columns under shear loading were investigated by Liu et al. (Liu et al., 2012), and observed that the joint stiffness and capacity is influenced by angle thickness and bolt gauge, but the experiment was conducted with hollow steel tube, and no CFST or extended hollo-bolts were involved. A recent study of extended hollo-bolt CFST joint under shear and combined shear and tensile forces was conducted by Pitrakkos et al. (Pitrakkos et al., 2021), and observed that highest ultimate strength of the hollo-bolt was obtained at a normalised tension-shear ratio of 30°. The study was conducted with single hollo-bolt and the influence of bolt embedment length was not considered. Since, in the existing works, only a very limited test were conducted on extended hollo-bolted CFST joints under shear, Debnath et al. (Debnath and Chan, 2022b) conducted a series of tests of single hollo-bolted CFST joints under predominant shear loading, and the parameters studied include, hollo-bolt embedment length, column cross-section, presence of infill and grade of concrete. The prominent observations were that the joint stiffness was improved by 80% due to infill concrete, with higher bolt embedment length the shear load was considerably transferred to the concrete core by bolt bearing, all the joints were able to achieve ultimate bolt capacity, and a predictive equation for shear strength was suggested. Now, as in an actual moment frame, the beam to CFST column joint will be fabricated with a group of hollo-bolts, it is further necessary to investigate the group effect of the bolts under shear loading.

In summary, it is observed from the existing studies that, most of the investigations on anchored hollo-bolted CFST column joints, under either monotonic or cyclic loadings, were based only on tensile performance, and studies on anchored blind-bolted composite column joints under shear loading are scarce. Since, in an actual moment frame, the joints will undergo both shear and bending forces, and as a result the hollo-bolts will experience combined tensile and shear forces, thus investigation of hollo-bolted CFST joints under shear forces is pertinent. The existing studies indicate that the extended hollo-bolt was able to display significantly higher performance under tensile loading, but further study is required to characterise its behaviour under shear loading. Further, it can be specifically stated that, there are visibly limited studies on group behavior of anchored blind-bolted CFST joints under shear loadings, and therefore, the current investigation will delve in to this aspect of the joints.

In the current study, a set of experimental test series is conducted for group of hollo-bolted CFST column joints under shear forces. For the study, group of two hollo-bolts and group of four hollo-bolts in a joint assembly have been considered. Other parameters studied include, number of bolt rows, hollo-bolt embedment length, and bolt pitch distance. A series of full-scale tests have been conducted in this testing program, followed by discussion on failure modes, global load-displacement behavior, and strain analysis which will help to develop further understanding of such joints. Lastly, the strength assessment of the joints was conducted, and experimental results were used to develop an analytical model to provide a fair prediction of the load-deformation behavior of hollo-bolted CFST joints under shear loading.

Research Framework

From the existing limited works, it is primarily evident that the extended hollo-bolts can be adopted for fabrication of joints that can offer semi-rigid or rigid joints. But for the development of hollo-bolted (blind-bolted) CFST column joints that can be adopted for moment-resisting frame, an extensive research program is required. Understanding of the joint behavior under various loading patterns is needed, and accordingly researchers have been conducting tests towards achieving the goal of developing design guidelines for extended hollo-bolted (or blind-bolted) CFST joints for international standards. It is also important to note that, few existing studies on anchored hollo-bolted beam-to-column joints that were conducted, had relatively thicker endplates, where joints failed by bolt fracture and exhibited semi-rigid behavior, and thus it remains to be investigated the joint performance that incorporates the influence of endplates, which would be closer to a real construction scenario. As a part of this research program, a testing program comprising of experimental, numerical and analytical studies is also being carried out at The Hong Kong Polytechnic University, and the research framework is shown in Figure 2. Initially, the hollo-bolted CFST joints under tensile forces have been carried out. The joints were fabricated with single hollo-bolt and groups of two and four hollo-bolts. Secondly, the testing program involved joints under predominant shear loading, where joints are fabricated with single and group of hollo-bolts. This paper presents the findings and observations of group of two and four hollo-bolts in a joint assembly. Further, the testing program will delve in to tensile behavior of hollo-bolted CFST joints with thin endplates, as previously the influence of endplate was ignored to understand the hollo-bolt performance. And lastly, the beam-to-CFST column joints fabricated with extended hollo-bolts can also be investigated under monotonic and cyclic loading to explore the moment-rotation behavior.

Experimental Investigation

Specimen Design and Labeling

To investigate the group behavior of the standard and hollo-bolts in CFST column joints, the specimens were designed having joints with group of two hollo-bolts and group of four hollo-bolts. For the laboratory testing program, eight specimens were developed for joints with two hollo-bolts, and five specimens were developed for joints with four hollo-bolts. Among these specimens, two specimens were also prepared to ensure repeatability and reliability of the test results. The steel tube section adopted for this testing program was of 250×250×6.3 mm, which is a typical column dimension used for multi-storey buildings. The length of all the specimens were 650 mm which was enough to eliminate the end boundary conditions for the hollo-bolted joints that will be subjected to shear forces. At the mid-height position, the steel tubes were provisioned with bolt holes on two opposite sides of the tube, and thus two hollo-bolted joints were fabricated for each specimen. This was done for the ease of shear load application to the joint without any overturning moment in the specimens. The upper end of the steel tube was kept open for concreting and the other end was closed by welding a thin plate to ensure no bleeding of fresh concrete. For the joint assembly, the endplates were made rigid by adopting a thickness of 40 mm, this was done to eliminate the influence of endplate in the global joint behavior. As one of the objectives of the testing program was to evaluate the performance of extended hollo-bolts in the CFST joints under shear loading, therefore it was necessary to overcome the influence of endplate. The alignment of the bolt holes in the steel tube and the bolt holes in the rigid endplate was maintained as closely as possible to avoid any misclosure. For fixing the hollo-bolts an electric wrench was used, and lastly a handheld torque wrench was used to apply the final torque in small increments and thereby apply the desired level of torque. The length of the hollo-bolts inside the steel tube is considered as the bolt embedment length. In this program three bolt embedment lengths were considered, $3.25d_b$, $4.6d_b$, and $5.35d_b$, where d_b is the hollo-bolt diameter. The hollo-bolts with embedment length $4.6d_b$, and $5.35d_b$ was attached with the headed nut, to provide anchorage in to the infill concrete. Three series of specimens were developed, where series B is referred to the test specimens having joints with two hollo-bolts arranged in single row. Specimens in series C is referred to test specimens having joints with two hollo-bolts arranged in two rows, and series D is referred to specimens having joints with four hollo-bolts arranged in two rows. The parameters studied in this experimental program include, number of hollo-bolts in the group, positioning of the hollo-bolts, pitch distance, and the bolt shank embedment length. The nomenclature used in this test program can be expressed as *B-Ex-Cy-Tz-R/P1,* where *B* refers to experimental series; *E* refers to bolt shank embedment length in millimeters; *C* refers to concrete grade in megapascals, *T* denotes steel tube wall thickness in millimetres; at the end; *R* denote repeated specimen, or *P1* denote different pitch distances of the hollo-bolt.

For all the specimens, wherever applicable, the pitch and gauge distance were kept at 2.85d_{hole} or 100 mm, where d_{hole} is bolt hole diameter, except for the specimens where influence of different pitch distance was examined had a pitch distance of 2.5d_{hole} or 90 mm. For example, the specimen B-E107-C40-T6.3-P1 refers to series B with bolt embedment length of 107 mm, with infill concrete of 40 MPa, tube thickness 6.3 mm and bolt pitch of 90 mm. The inside view of the specimen series B, C and D is shown in Figure 3. The geometric dimensions of the steel tube and hollo-bolt and other information are presented in Table 1 and Table 2. For the fabrication of the specimens, initially the steel tubes were prepared with required number of bolt holes on two opposite sides of the tube. The joints were then developed by placing the hollo-bolts through the rigid endplate coinciding with the tube holes. The bottom side of the tube had welded steel plate to avoid any water leakage after pouring fresh concrete. The alignment of the bolt holes and the rigid plate holes were maintained in the best possible way to avoid any misclosure. After tightening the hollo-bolts with the desired torque level, the specimens were made ready for concreting. After concreting, the open end of the specimens was covered with cling film wrap to avoid direct air contact. For the positioning of the blind-bolt holes, the references to the minimum and maximum spacing, end and edge distances provided in the Eurocode 3 Part 1-8 (CEN, 2005) is made. For the blind-bolts, high-strength bolts of class of 8.8 with adequate preloading with controlled tightening was adopted.

Laboratory Test Setup

The testing program was conducted with MTS 815 Rock Mechanic testing system, which has a capacity of 4600 kN, with the bottom crosshead travel of ± 50 mm. As support base plate was fabricated to be placed on the bottom crosshead of the testing system, on which the CFST column specimens were mounted. To apply the shear load to the hollo-bolted joints, an inverted U-frame was designed with high strength steel, that will remain elastic under the applied load. The frame was placed carefully above the joint rigid plates on two sides of the CFST column, and the stability of the frame was ensured. A compression platen was placed between the inverted U-frame and the load cell of the MTS machine to ensure uniform loading to the specimen. For the specimens having joints with two bolts a preload of 15 kN, and for the specimens having joints with four bolts a preload of 30 kN was applied. This was done to check for any instabilities in the setup and also the functioning of the instrumentations. A loading rate of 0.3 mm/min was maintained for all the specimens in the experimental program. The three-dimensional schematic diagram of the test setup and the actual experimental test setup using the MTS testing system is presented in Figure 4 and Figure 5, respectively.

Instrumentation

Three Linear variable differential transducers (LVDTs) were used to measure the displacement of the hollo-bolted joints, where two LVDTs (L1 and L2) were placed on the movable crosshead of the MTS testing system to record the joint displacement, and the other LVDT (L3) was attached to the rigid plate at the joint to monitor any displacement in the reaction frame. During the analysis of the results, the average recording of L1 and L2 were used to obtain the final deformation of the joints, assuming that the load was applied equally on the joints in both the sides of the CFST column. Strain gauges were used to measure the steel tube strain and the bolt strain. For the steel tube, the strain gauges were placed just below the bolt holes, to capture the local strain developed in the steel tube. The tube strain gauges are referred here as TSG. For the bolt strain gauges, they were placed on the shank, at the location closest to the headed nut.

As the hollo-bolts under the shear loading will possibly undergo bending forces, where the upper region of the bolt shank will experience tensile forces, and the lower region will experience compressive forces, therefore two strain gauges were applied for each bolt shank, to record both the forces developed in the shank. The strain gauges attached to the bolt shank are referred to as BSG. For the strain gauges attached to the bolt shank, water proofing was applied and also covered with coating tape to protect them from infill fresh concrete. It is important to note that, strain gauges were not fixed on the standard hollo-bolts due to insufficient bolt shank length, and thus were applied only to extended hollo-bolts. The positioning of the LVDTs and strain gauges in the specimen in shown in Figure 6.

Material tests

The steel tubes of CFST column were fabricated from S355 grade hot-rolled steel plates, having thickness of 6.3 mm. For determining the mechanical properties of the steel tube, flat dog-bone shaped coupons were curved out whose dimensions were designed as per ISO 6892-1:2019(EN) (ISO, 2019). Similarly, for determining the mechanical properties of the M20 hollo-bolts, three coupons from each batch of bolt shank were considered. This was done as three different embedment length of 65 mm, 92 mm, and 107 mm of hollo-bolts shank belonged to actual shank length of 120 mm, 150 mm, and 165 mm, respectively, which were from three different batches. That is, a total of nine circular bolt shank coupons were designed and tested at loading rate of 0.02 mm/min until a strain of 1% was reached, 0.2 mm/min loading rate was used from 1% strain to 7% strain, and beyond 7% strain a loading rate of 0.5 mm/min was used. The Instron UTM machine was used to test the steel flat coupon and bolt circular coupons, the setup of which is presented in Figure 7. During the material tests, apart from clip extensometers for measuring the displacement, strain gauges were also used to accurately measure the elastic modulus. Rockwell hardness testing machine was used to measure the strength values of hollo-bolt expandable sleeve. The measured material properties of steel tubes, bolt shank and bolt sleeve are presented in Table 3. For the infill concrete, grade of C40/50 which is usually used for regular construction was adopted. For this experimental program, the commercial concrete was used. For the mix, water to cement ratio of 0.54 was used, along with superplasticizer of 2.5 kg/m^3. A slump of 125 mm was achieved. To test the compressive and split tensile strength of the concrete cylinders of size 100 mm diameter and 200 mm length were casted. Strain gauges were applied on the cylinders to accurately measure the elastic modulus. The cylinder average compressive strength, split tensile strength and the elastic modulus obtained were 39.1 MPa, 3.45 MPa, and 26500 MPa, respectively.

Results and Discussions

Failure Mode and General Behavior

The observed failure modes and the global behavior of the CFST hollo-bolted joints are discussed in this section. For the specimens in Series B, the joints were fabricated using two hollo-bolts, arranged in single row and two columns. For the specimen B-E65-C40-T6.3, the failure mode was by total shear fracture of the hollo-bolt, where initially the bolt sleeve deforms by bending, and upon touching the bolt shank the load is transferred to the shank. A cracking sound at about 180 kN was heard, which possibly could be due to failure of the sleeve. Upon total shear fracture of the bolts, the joint got separated from the CFST column, and the test was ceased. Similarly, for the specimen B-E92-C40-T6.3, where the bolt embedment length was 92 mm, a cracking sound was heard at 230 kN, with a possible indication of failure of the sleeve. Upon applying further loading and after achieving peak load, the specimen had the global failure mode of hollo-bolt shear fracture and ultimately separated from the CFST column. The repeated specimen B-E92-C40-T6.3-R had the same failure mode as B-E92-C40-T6.3, thus confirming the reliability of the test. For the specimen B-E107-C40-T6.3 having a bolt embedment length of 107 mm, failure was governed by shear fracture of the hollo-bolts, leading to the joint failure in shear. The specimens after test are shown in Figure 8(a) and Figure 8(b) for the specimens B-E92-C40-T6.3-R and B-E107-C40-T6.3, and the sheared-off hollo-bolts are shown in Figure 8(c). To investigate the influence of bolt pitch distance on the joint behavior, the specimen B-E107-C40-T6.3-P1 was fabricated, with a pitch distance of $2.5d_{hole}$ or 90 mm, unlike remaining specimens having pitch distance of $2.85d_{hole}$ or 100 mm. A similar mode of joint failure by bolt shear fracture occurred, and the reduction in pitch length had negligible influence, as observed within the studied limit. For further investigation of the tested specimens, the steel tube was removed from the joint region to investigate the possible damage in the confined concrete. Upon inspection, it was observed that there were minor cracks around the hollo-bolt and the crack propagated only for a short length of about 6 to 7 mm. There was no visible bearing failure in the concrete. Under the applied loading, as the shear load also transmitted to the steel tube, there was visible local bulging of the steel tube just beneath the bolt hole. The condition of the infill concrete and the bulged steel tube is shown in Figure 9.

For the specimens in Series C, the CFST joints were fabricated with two hollo-bolts, arranged in single column and two rows, with bolt gauge distance of $2.85d_{hole}$, that is,100 mm. The specimens C-E65-C40-T6.3, C-E92-C40-T6.3 and C-E107-C40-T6.3 were fabricated where three different hollo-bolt embedment lengths of $3.25d_b$, $4.6d_b$, and $5.35d_b$, respectively were tested. The failure modes of the specimens were also governed by shear fracture of hollo-bolt, and no prominent concrete cracking were noticed. For all the three specimens, the rigid end plate with the sheared-off portion of the hollo-bolts were detached from the CFST column upon reaching the failure load. Upon removal of the steel tube portion from the joint region, there was no signs of concrete bearing failure, except some micro cracks generated around the bolt hole. The specimens after test is shown in Figure 10.

As a next step forward, the experimental investigation was further extended to study the influence of group of four hollo-bolts in the CFST joint behavior. The specimens in this series D was fabricated by four hollo-bolts, arranged in two rows and two columns. The specimen D-E65-C40-T6.3 failed by bolt shear fracture, leading to separation of the rigid end plate and the sheared-off hollo-bolt portions from the column. It should be noted that, the other joint of the specimen D-E65-C40-T6.3 did not shear-off at the same load, possibly due to some unequal loading applied to the joint due to alignment issues. The specimens with longer bolt embedment depths, D-E92-C40-T6.3, D-E92-C40-T6.3-R and D-E107-C40-T6.3 also had similar joint failure mode. Also, in this series of tests, the influence of hollo-bolt pitch distance was investigated, and accordingly the specimen D-E107-C40-T6.3-P1 was fabricated with pitch distance of $2.5d_{\text{hole}}$. It was noted that this specimen under had some unequal displacements at around the load of 1200 kN, possibly initiating the concrete cracking in either side of the joints, and followed by cracking sounds at about 1740 kN, possibly due to further concrete cracks. The specimen ultimately failed by shear fracture of the hollo-bolts. Due to presence of four hollo-bolts in the joint assembly, it was expected to have significant concrete crushing followed by concrete bearing failure. To examine this fact, the steel tube was removed from the joint area for two specimens D-E92-C40-T6.3 and D-E107-C40-T6.3-P1. It was noted that some cracks were visible around the bolts in the upper region, and moreover for the specimen D-E107-C40-T6.3-P1 the cracks between the bolts in the upper region was slightly intensified as compared to D-E92-C40-T6.3. This is possibly due to reduced pitch distance between the extended hollo-bolts leading to overlapping of stresses in the specimen D-E107-C40-T6.3-P1. The specimens after test and the concrete cracks generated for the specimens in series D are represented in Figure 11. It is to be noted that, though there were some prominent concrete cracks in these specimens, there were no failure of the joints by concrete bearing.

Force-Displacement Behavior

The global load-displacement behavior of the hollo-bolted CFST column joints under shear loading are presented in this section. The plots for the load-displacement behavior are measured based on the LVDT movement and load cell attached to MTS rock mechanic system. The presented load values refer to force per joint, that is, total applied load to the specimen was twice the load per joint. Apart from the attained peak load, the joint stiffness was also calculated from these plots. The stiffness offered from the expandable sleeve was considered as the initial stiffness k, which can be measured at about 15% of the peak load. As the load is gradually transmitted to the bolt shank, the stiffness measured at 70% of the peak load can be considered as the joint stiffness, and can be referred as k_{sc}. The measure of stiffness at 70% of ultimate resistance is also recommended by Eurocode 4 (CEN, 2009). Figure 12 presents the load-deformation behavior for series B specimens. Figure 12 (a) presents the load-displacement behavior for the specimens B-E65-C40-T6.3 and B-E92-C40-T6.3 having bolt embedment length of $3.25d_b$ and $4.6d_b$, respectively. The peak loads achieved for B-E65-C40-T6.3 and B-E92-C40-T6.3 were 462 kN and 510.5 kN, with initial stiffness of 77.36 kN/mm and 84.28 kN/mm, respectively. The 10% increase in strength for the specimen B-E92-C40-T6.3 was observed as the bolt shank of length 150 mm was used for this specimen, which had higher mechanical capacity as can be referred from Table 3. Further, the repeated specimen B-E92-C40-T6.3-R is plotted with B-E92-C40-T6.3 to confirm the repeatability of the test results, which shows the stiffness and peak load are in good agreement with each other and can be referred from Figure 12 (b). The specimen B-E107-C40-T6.3 with higher bolt embedment length of 5.35d_b achieved peak load of 528 kN, which is a slight increase of 3.5% as compared to the B-E92-C40-T6.3, as shown in Figure 12 (c). For the specimen B-E107-C40-T6.3-P1 having reduced pitch of 90 mm attained a peak load of 565 kN, but with a reduced stiffness of 66.63 kN/mm as shown in Figure 12 (d). The load-deformation behavior for the specimens in series C are presented in Figure 13. As can be referred from Figure 13 (a) and Figure 13 (b), the peak loads achieved by the specimens C-E65-C40-T6.3, C-E92-C40-T6.3 and C-E107-C40-T6.3 are 490 kN, 500.5 kN and 498.5 kN, respectively, thus indicating that within the studied parameters, the increase in embedment length did not alter the load carrying capacity of the joints as when the two hollo-bolts in the joint assembly were arranged in one column and two rows.

For the test specimens in series D, where joints were fabricated with four hollo-bolts are presented in Figure 14. In these specimens, the primary focus was also to investigate the group effect of the hollo-bolts, that has three different embedment lengths of 3.25d_b, 4.6d_b and 5.35d_b. The specimen D-E65-C40-T6.3 and D-E92-C40-T6.3 attained peak loads of 1052 kN and 1060.5 kN, respectively, as shown in Figure 14 (a). The repeated specimen D-E92-C40-T6.3-R achieved the peak load of 1056 kN showing good agreement with D-E92-C40-T6.3, as presented in Figure 14 (b). When compared with specimen D-E107-C40-T6.3 having embedment length 5.35d_b, the load achieved was 960 kN, which is about 10.5% less than D-E92-C40-T6.3, as shown in Figure 14 (c). This was due to higher mechanical strength of bolt shank of length 150 mm which was used for D-E92-C40-T6.3, as can be referred from Table 3.

The specimen D-E107-C40-T6.3-P1 with reduced pitch distance of 90 mm was also compared with D-E107-C40-T6.3, which displayed similar load-deformation behavior as seen in Figure 14 (d). As can be also inferred from Figure 14, the influence of expandable sleeve diminishes in global behavior of joint, as compared to the joints which were fabricated with single hollo-bolt (Debnath and Chan, 2022b) and double hollo-bolts (series B and C, in this article), where the initial stiffness was influenced by the sleeve deformation. As can be referred from the force-displacement curves, for most of the specimens in all the three series, the typical force-displacement curve increases gradually to reach the maximum force ($F_{\mathrm{v,max}}$) and beyond which this force is retained for a displacement of approximately 1.5 to 2 mm, before finally shearing-off. The peak force ($F_{\mathrm{v,max}}$), displacement at the peak force (S_{u}), ultimate displacement ($S_{\max}$), stiffness (k) and failure mode of the tested CFST hollo-bolted joints are presented in Table 4.

Strain Analysis

The strain measured in the extended hollo-bolts and steel tube surface are discussed here. Strain gauges were attached to the extended hollo-bolts on two sides at 180° of each other, intended to measure the stain developed at the region close to the headed nut. The portion of the bolt shank which is embedded into the concrete core will undergo bending forces, and as a result the upper region of the shank will experience tensile forces, whilst the lower region of the shank will experience compressive forces. The strain developed in the bolt can be referred from the representative Figure 15, where the positive strain refers to tensile forces in the upper region of the shank and the negative strain corresponds to compressive forces in the lower region of the shank. It can be noted that, the strain reached the concrete strain at peak stress of approximately 2800 με, indicating effective transfer of the shear load via the embedded hollo-bolt. This also signifies the concrete contribution in transferring the applied load. Similar trends were observed for the specimens having bolt embedment length of $3.25d_{\mathrm{b}}$, $4.6d_{\mathrm{b}}$ and $5.35d_{\mathrm{b}}$ for all the series of specimens. This strain data can also be used to measure the stress developed in the concrete region and thereby calculate the load borne by the infill concrete by bearing, and the remaining load being transferred by the steel tube. As referred from Figure 15 (a), for the series B specimens, in a joint both the bolts are located at the same level and demonstrates similar amount of strain, and thus the applied load can be assumed to be distributed equally to all the hollo-bolts. It can be concluded that for the specimens with embedment length of $4.6d_b$ and $5.35d_b$ about 52% of the shear load was transferred to the concrete infill, signifying enhanced composite behavior of the CFST columns due to elongated bolt shanks.

But for the specimens in series C, in a joint the hollo-bolts were positioned at two levels, and as can be referred from Figure 15 (b), the amount of strain developed are very close for the hollo-bolts at the same level, whereas, the hollo-bolts at the lower level developed lesser strain as compared to the bolts in upper level. The extended hollo-bolts at the upper level had almost double the strain (approximately 2000με) as compared to the extended hollo-bolts in the lower level (approximately 1100 με). This indicates that the extended hollo-bolts in the upper level has transmitted higher load to the concrete core as compared to the extended hollo-bolts in the lower level. This remains to be mentioned that, after applying the final bolt torque during fabrication, the position of few bolt strain gauges could not be exactly maintained at the desired position to measure the compressive and tensile strain in the bolt shank. And possibly therefore, some deviation arises in the bolt strain measurements at the same level, say in Fig. 15 (b), between BSG 1 and BSG 5, and between BSG 3 and BSG 7. A similar pattern was also observed for the specimens in Series D, where in a joint four extended hollo-bolts were positioned at two levels, where the two hollo-bolts at the upper level developed more strain as compared to the hollo-bolts at the lower level. From the strain data assessment, the upper row extended hollo-bolts was able to distribute approximately 40% of the shear load to the concrete core, and the second row extended hollo-bolts could distribute about 25% of the shear force to the concrete core. This trend also indicates that, the co-efficient of shear force borne by the concrete through bearing of extended hollo-bolts positioned at upper rows will be high as compared to lower rows. The remaining force is transferred by the steel tube, which is 6.3mm thickness in the current study. Further investigation needs to be conducted with higher *B/t* ratio for enhanced concrete contribution. The localised strain below the bolt hole as measured is represented in Figure 16, which shows that bolt embedment length does not significantly influence the tube strain under pure shear loading. As observed from the failure modes of the hollo-bolted CFST joints under the shear loadings, the joints show irreversible damage, where both the shank and the expandable sleeve have undergone shear fracture. Therefore, to ensure life-cycle resilience of such structural components, self-centering technologies like shape memory alloy-based components can be adopted (Hu et al., 2023b, Hu and Zhu, 2023).

Strength Assessment

Expression of Force-Displacement Relationship

As discussed in the introduction, that in a hollo-bolted CFST joint, the hollo-bolts will usually experience both tensile and shear forces, and thus it is necessary to evaluate the behaviour of the joint under individual forces. Therefore, to conservatively predict the stiffness, strength and ductility for design and analysis of hollo-bolted CFST column joints under shear loading, a suitable force-displacement relationship model is required to be established. Since there are very limited observations in the literature on the shear performance of hollo-bolted CFST joints and thus no existing models are available, therefore, for the development of a force-displacement model, previous observations on headed shear stud connectors in composite beams have been referred. The static behavior and the corresponding theoretical model developed by Xue et al. (Xue et al., 2008) for stud shear connectors under push-out loading, where most of the tests failed by shank failure irrespective of stud dimension and concrete grade, was analysed for its suitability in the current testing program where similar failure mode of bolt shank failure was observed. The model developed by Xue et al. (Xue et al., 2008) was based on push-out test results and analysis of existing empirical equations, and a similar expression was adopted to fit the current test data as presented in equation (1).

$$\frac{F_{\mathrm{v}}}{F_{\mathrm{v,max}}} = \frac{0.67x}{3+0.36x} \tag{1}$$

where x = joint displacement in millimeters, along the direction of applied shear force.

The curve developed based on equation 1 is presented in Fig. 17, where the normalized force versus joint displacement is plotted, and compared with the sample test result. As can be noted from Fig. 17, the function when compared to the typical measured force-displacement curve, it is not able to provide a fair prediction of the global behaviour, estimating the stiffness with a convex shape, and is unable to capture the post-peak behavior of the hollo-bolted CFST joints.

Therefore, based on the experimental test results and as observed from the force-displacement behavior of the tested specimens in series B, C and D, the joints with different hollo-bolt embedment depth, pitch distance and bolt row arrangement have curves of same shape, and thus the global behavior can be predicted from a new empirical relationship, based on curve-fitting, which is given as follows:

$$\frac{F_{\mathrm{v}}}{F_{\mathrm{v,max}}} = -0.2 + 1.2\, e^{\frac{-(x-8)^2}{36}} \tag{2}$$

where x = joint displacement in millimeters, along the direction of applied shear force.

As can be seen from Fig. 17, the derived simplified model in equation (2) have a better agreement of the force-displacement relationship for the hollo-bolted CFST column joints under shear loading. The comparison of the experimental and analytical curves is made in Fig. 18 (a) for the specimens in series B and C, and in Fig. 18 (b) for specimens of series D, and it can be noted that the proposed model can fairly predict the force-displacement response for all the tested specimens. It must be mentioned that test results of a few specimens, D-E65-C40-T6.3, D-E92-C40-T6.3 and D-E92-C40-T6.3-R show lesser stiffness than the proposed model beyond $0.6F_{\mathrm{v}}/F_{\mathrm{v,max}}$, because the proposed model is based on calibration of all data including series B and C, thereby to develop a general equation to represent the force-displacement behavior of CFST joints with groups of two and four hollo-bolts under shear loading.

Table 5 presents the comparison of the calculated and measured values, where it can be observed that the mean value for ratio of measured to calculated values for normalized force of 0.5 is 0.86 with CoV as 0.02, and at a normalized force of 1.0 the mean value is 1.13 with CoV as 0.01, indicating a good estimation of the force-displacement relationship. As seen from Fig. 18 and Table 5, that based on the observed failure mode, a single equation is able to represent the force-displacement behavior of the hollo-bolted CFST joints with different arrangement of bolts in group, it also remains to be analysed the possibilities of other failure modes, like concrete crushing and end plate bearing failure, and necessity of developing any further predictive equations.

Expression of Joint Capacity

As no international design codes are currently available for blind-bolted joints to composite structures, therefore to determine the shear strength of joints fabricated with hollo-bolts anchored in the CFST column the American building code (ACI318-19, 2019) is referred. The ACI 318-19 provides the shear strength for steel strength of anchors and concrete breakout strength under shear loading for structures where steel headed bolt or hooked bolts are anchored in concrete with open edges. The steel strength of anchors in shear, F_{sa} is given in Equation (3):

$$F_{\mathrm{sa}} = 0.6\, A_{\mathrm{se,V}}\, f_{\mathrm{uta}} \tag{3}$$

where $A_{\mathrm{se,V}}$ = effective cross-sectional area of an anchor in shear; and f_{uta} = specified strength of anchor steel. The concrete breakout strength, V_{cbg} in shear of group of anchors is given by Equation (4):

$$V_{\text{cbg}} = \frac{A_{\text{vc}}}{A_{Vco}} \Psi_{\text{n}} V_{\text{b}} \tag{4}$$

where A_{vc} = projected concrete failure area of the steel anchor group and is approximated by a rectangle with edges bounded by 1.5 times the edge distance of concrete in the direction of the shear force; and A_{Vco} = total projected shear failure area approximated by a square bounded by 1.5 times the edge distance from the centreline of the anchor in all sides. Ψ_{n} is refereed here in short form that represents different modification factors that include eccentricity, edge effect and concrete cracking; and V_{b} is the basic concrete break out strength of single anchor in shear. V_{b} is given by:

$$V_{\text{b}} = \left(7\left(\frac{l_e}{d_a}\right)^{0.2}\sqrt{d_a}\right)\lambda_a\sqrt{f_c'}(c_{a1})^{1.5} \tag{5}$$

where l_e = load bearing length of the anchor in shear; d_a = diameter of the anchor bolt; λ_a = factor for reduced concrete mechanical properties if lightweight concrete was used; and f_c' = cylinder compressive strength of concrete. The ACI318-19 also has provisions for anchors in narrow member of limited thickness. But both the above equations (3) and (4) could not be applied to determine the shear strength of group anchored hollo-bolted CFST column joints as no concrete breakout strength was observed in the current experimental program. This can be attributed to the high confinement provided to the infill concrete on the edges by the steel tube, and as a result, all the joints failed by hollo-bolt shear failure. As reported previously (Debnath and Chan, 2022b), the shear resistance of single standard and extended hollo-bolt having joint in CFST columns can be modified to predict a conservative value as presented in the following equation:

$$F_{\text{v, max}} = 0.55\,(f_{\text{u,b}} A_{\text{t}} + f_{\text{u,sl}} A_{\text{sl}}) \tag{6}$$

where $f_{\text{u,b}}$ = bolt ultimate tensile strength; A_{t} = tensile stress area of bolt shank; $f_{\text{u,sl}}$ = sleeve ultimate strength; and A_{sl} = net sleeve area of the hollo-bolt.

This equation was standalone proposed for strength prediction as no concrete pry out, breakout or bearing failure was observed. Also, it is observed from the current experimental program of pure shear loading in joints fabricated with group of standard and extended hollo-bolts in CFST column, all the joints failed by bolt shear fracture, and no prominent concrete breakout was reported. For all the specimens where the bolts were arranged in groups of two bolts in series B and C; and group of four bolts in series D, the hollo-bolts possibly behaved as individual bolts and thus the joint capacities can be calculated by equation (6) multiplied by the number of bolts, *n*, in the joint assembly. This can be confirmed from Table 5, where the mean value of test results to predicted maximum joint shear capacity based on the hollo-bolt strength (Measured $F_{\mathrm{v,max}}$) / (Calculated $F_{\mathrm{v,max}}$) obtained is 1.03.

Further, all the CFST joints with group of two and four hollo-bolts adopted in the study were able to attain the maximum capacity of the hollo-bolts. Within the studied parameters and limitations in this work, the design shear resistance of the anchored hollo-bolted joints can be taken as the following:

$$F_{\mathrm{v,Rd}} = n\frac{\alpha_b\,(f_{\mathrm{u,b}}\,A_{\mathrm{t}} + f_{\mathrm{u,sl}}\,A_{\mathrm{sl}})}{\gamma_{M2}} \tag{7}$$

Where:

α_b = 0.55 for anchor blind-bolts having shank and sleeve yield strength 800 N/mm^2 and 390 N/mm^2, respectively; *n* = number of bolts in the assembly; and γ_{M2} = partial safety factor as per Eurocode (CEN, 2005).

It should be noted that, the strength prediction of the joints can also be influenced by the inherent uncertainties of the materials and geometries (Hu et al., 2022, Hu et al., 2023a). Therefore, this aspect can be considered in future studies to incorporate the uncertainties of the structural components in joint strength prediction.

Conclusions

An experimental program was conducted to explore the shear performance of group hollo-bolted CFST column joints. The joints were designed with group of two hollo-bolts and four hollo-bolts, and the parameters studied include, bolt shank embedment length, bolt rows arrangement, and bolt pitch distance. In order to assess the joint behavior, a total of 13 full-scale tests were conducted, and the failure patterns, shear resistance including load-deformation curves, strain analysis and joint strength analysis have been conducted in detail. The following key observations are presented here:

1. All the CFST column joints fabricated with group of two hollo-bolts and four hollo-bolts, enhanced concrete contribution in shear load transfer was observed with higher bolt embedment length, but the joint failure mode and joint strength is not influenced by the bolt shank embedment length and the bolt pitch distance.

2. For the series B tests, where joints fabricated with group of two hollo-bolts at the same level, the shear force can be assumed to be distributed equally to all the bolts, and specimen having embedment of $4.6d_{\mathrm{b}}$ and $5.35d_{\mathrm{b}}$ can transfer up to 52% of the shear force to the concrete core. For the series C and D tests, where joints fabricated with group of two hollo-bolts at two levels, the extended hollo-bolt at the upper level transfers more shear forces to the concrete core (about 40%) as compared to the extended hollo-bolt at the lower level (about 25%).

3. In the tests, hollo-bolt shear fracture has been the prominent failure mode, and no significant concrete crushing damage was observed. This indicates that, though the joints were fabricated with group of standard and anchored hollo-bolts, but behaved as individual hollo-bolts and the tests were able to achieve the ultimate capacity of the hollo-bolts. Within the studied limit, it can be

stated that pitch distance beyond $2.5d_{\text{hole}}$, the total strength of the joint was equal to sum of shear strength of individual bolts, which confirms that the group action does not influence the strength.

4. An expression for force-displacement relationship and joint bearing capacity has been proposed that can well predict the global behavior of the hollo-bolted CFST joints under shear load within the test matrix investigated in this research.

Due to limited resources, the study predominantly focused only one column cross-section and group of hollo-bolts in two rows only. As in the current study, a compact steel tube section was adopted and thus a significant amount of shear force was borne by the tube wall, therefore further investigation needs to be conducted with higher *B/t* ratio (non-compact and slender sections) for enhanced concrete contribution in load transfer. Joints with more rows of hollo-bolt and closer pitch distance also needs to be investigated to further investigate any possibilities of bolt group effect, and find out the co-efficient of shear load taken by each row. Further to this, to anchored blind-bolted CFST column-to-beam joints with non-rigid end plates need to be conducted to fully understand the influence of all the members of the joint assembly. Future works in this domain can be expanded by incorporating inherent uncertainties of the structural components in strength prediction and, adopting self-centering technologies to enhance the joint resilience.

Acknowledgement

The support received from the Chinese National Engineering Research Centre for Steel Construction (Hong Kong Branch) at The Hong Kong Polytechnic University is duly acknowledged.

Data Availability Statement

Some or all data, models, or codes that support the findings of this study are available from the corresponding author upon reasonable request.

References

ABRAMSKI, M. 2018. Load-carrying capacity of axially loaded concrete-filled steel tubular columns made of thin tubes. *Archives of Civil and Mechanical Engineering,* 18**,** 902-913.

ACI318-19 2019. Building Codes Requirements for Structural Concrete (ACI 318-19).

AGHESHLUI, H., GOLDSWORTHY, H., GAD, E. & FERNANDO, S. 2016a. Tensile behaviour of anchored blind bolts in concrete filled square hollow sections. *Materials and Structures,* 49**,** 1511-1525.

AGHESHLUI, H., GOLDSWORTHY, H., GAD, E. & YAO, H. 2016b. Tensile Behavior of Groups of Anchored Blind Bolts within Concrete-Filled Steel Square Hollow Sections. *Journal of Structural Engineering,* 142**,** 04015125.

AJAX 2002. ONESIDE brochure B-N012 data sheet. Melbourne, VIC, Australia: AJAX Engineered Fasteners.

CABRERA, M., TIZANI, W., MAHMOOD, M. & SHAMSUDIN, M. F. 2020. Analysis of Extended Hollo-Bolt connections: Combined failure in tension. *Journal of Constructional Steel Research,* 165**,** 105766.

CEN 2005. Eurocode 3 : Design of Steel Structures- Part 1-8: Design of Joints. BS EN 1993-1-8: 2005.

CEN 2009. EN 1994-1-1, Eurocode 4: Design of Composite Steel and Concrete Structures – Part 1-1: General Rules and Rules for Buildings.

CHEN, J., CHAN, T.-M. & CHUNG, K.-F. 2021. Design of square and rectangular CFST cross-sectional capacities in compression. *Journal of Constructional Steel Research,* 176**,** 106419.

DEBNATH, P. P. & CHAN, T.-M. 2021a. A comprehensive numerical approach for modelling blind-bolted CFST connections. *Structures*, 33, 2208-2225.

DEBNATH, P. P. & CHAN, T.-M. 2021b. Tensile behaviour of headed anchored hollo-bolts in concrete filled hollow steel tube connections. *Engineering Structures,* 234, 111982.

DEBNATH, P. P. & CHAN, T.-M. 2022a. Experimental evaluation and component model for single anchored blind-bolted concrete filled tube connections under direct tension. *Journal of Constructional Steel Research,* 196, 107391.

DEBNATH, P. P. & CHAN, T.-M. 2022b. Experimental performance of single blind-bolted CFST column connection under predominant shear loading. *Journal of Constructional Steel Research,* 196, 107386.

DEBNATH, P. P., XU, F. & CHAN, T.-M. 2023. Load transfer mechanism in concrete-filled steel tubular columns: Developments, challenges and opportunities. *Journal of Constructional Steel Research*, 107781.

FANG, H., CHAN, T.-M. & YOUNG, B. 2021. Structural performance of concrete-filled cold-formed high-strength steel octagonal tubular stub columns. *Engineering Structures,* 239, 112360.

GAO, X., WANG, W., TEH, L. H. & ZHUANG, L. 2022. A novel slip-critical blind bolt: Experimental studies on shear, tensile and combined tensile–shear resistances. *Thin-Walled Structures,* 170, 108630.

GOLDSWORTHY, H. M. & GARDNER, A. P. 2006. Feasibility study for blind-bolted connections to concrete-filled circular steel tubular columns. *Structural Engineering and Mechanics,* 24, 463-478.

HU, S., WANG, W. & LIN, X. 2022. Two-stage machine learning framework for developing probabilistic strength prediction models of structural components: An application for RHS-CHS T-joint. *Engineering Structures,* 266, 114548.

HU, S., WANG, W. & LU, Y. 2023a. Explainable machine learning models for probabilistic buckling stress prediction of steel shear panel dampers. *Engineering Structures,* 288, 116235.

HU, S., WANG, W., SHAHRIA ALAM, M. & KE, K. 2023b. Life-cycle benefits estimation of self-centering building structures. *Engineering Structures,* 284, 115982.

HU, S. & ZHU, S. 2023. Life-cycle benefits estimation for hybrid seismic-resistant self-centering braced frames. *Earthquake Engineering & Structural Dynamics,* 52, 3097-3119.

ISO 2019. British Standards Institution 6892-1:2019(EN)

Metallic materials — Tensile testing — Part 1: Method of test at room temperature.

JEDDI, M. Z. & SULONG, N. H. R. 2018. Pull-out performance of a novel anchor blind bolt (TubeBolt) for beam to concrete-filled tubular (CFT) column bolted connections. *Thin-Walled Structures,* 124, 402-414.

JIANG, J., ZHANG, J., LIU, J., CHIEW, S. P. & LEE, C. K. 2018. Effect of welding and heat treatment on strength of high-strength steel columns. *Journal of Constructional Steel Research,* 151, 238-252.

JIAO, W., WANG, W., CHEN, Y. & TEH, L. H. 2020. Seismic performance of concrete-filled SHS column-to-beam connections with slip-critical blind bolts. *Journal of Constructional Steel Research,* 170, 106075.

LINDAPTER 2018. Brochure of Hollo-Bolt by Lindapter, Bradford, UK.

LIU, M., ZHANG, B., LIU, Q., LIU, Y., TANG, L., ZHANG, W., LIU, F. & WANG, P. 2021. Experimental studies on thread-fixed one-side bolted endplate connection with internal strengthening structure. *Engineering Structures,* 246**,** 112977.

LIU, Y., MÁLAGA-CHUQUITAYPE, C. & ELGHAZOULI, A. Y. 2012. Behaviour of beam-to-tubular column angle connections under shear loads. *Engineering Structures,* 42**,** 434-456.

OKTAVIANUS, Y., GOLDSWORTHY, H. M. & GAD, E. 2017a. Group Behavior of Double-Headed Anchored Blind Bolts within Concrete-Filled Circular Hollow Sections under Cyclic Loading. *Journal of Structural Engineering,* 143.

OKTAVIANUS, Y., GOLDSWORTHY, H. M. & GAD, E. F. 2017b. Cyclic behaviour of individual double headed anchored blind bolts within CFST. *Journal of Constructional Steel Research,* 133**,** 522-534.

PITRAKKOS, T. & TIZANI, W. 2013. Experimental behaviour of a novel anchored blind-bolt in tension. *Engineering Structures,* 49**,** 905-919.

PITRAKKOS, T., TIZANI, W., CABRERA, M. & FAQE SALH, N. 2021. Blind bolts with headed anchors under combined tension and shear. *Journal of Constructional Steel Research,* 179**,** 106546.

POKHAREL, T., GOLDSWORTHY, H. M. & GAD, E. F. 2021. Tensile Behavior of Groups of Double-Headed Anchored Blind Bolts within Concrete-Filled Square Hollow Sections under Cyclic Loading. *Journal of Structural Engineering,* 147**,** 04020349.

SUN, L., LIANG, Z., WANG, Q., ZHU, H., WANG, P., LIU, Y. & LIU, F. 2021. Seismic response on T-head square-neck one-side bolted endplate connection of beam to square tubular column. *Engineering Structures,* 246**,** 113077.

SUN, L., LIU, M., LIU, Y., WANG, P., ZHAO, H., SUN, J. & SHANG, Y. 2020. Studies on T-shaped one-side bolted connection to hollow section column under bending. *Journal of Constructional Steel Research,* 175, 106359.

THAI, H.-T., UY, B., YAMESRI & ASLANI, F. 2017. Behaviour of bolted endplate composite joints to square and circular CFST columns. *Journal of Constructional Steel Research,* 131, 68-82.

TIZANI, W., AL-MUGHAIRI, A., OWEN, J. S. & PITRAKKOS, T. 2013a. Rotational stiffness of a blind-bolted connection to concrete-filled tubes using modified Hollo-bolt. *Journal of Constructional Steel Research,* 80, 317-331.

TIZANI, W., MAHMOOD, M. & BOURNAS, D. 2020. Effect of Concrete Infill and Slenderness on Column-Face Component in Anchored Blind-Bolt Connections. *Journal of Structural Engineering,* 146, 04020041.

TIZANI, W. & PITRAKKOS, T. 2015. Performance of T-Stub to CFT Joints Using Blind Bolts with Headed Anchors. *Journal of Structural Engineering,* 141, 04015001.

TIZANI, W., RAHMAN, N. A. & PITRAKKOS, T. 2014. Fatigue life of an anchored blind-bolt loaded in tension. *Journal of Constructional Steel Research,* 93, 1-8.

TIZANI, W., WANG, Z. Y. & HAJIRASOULIHA, I. 2013b. Hysteretic performance of a new blind bolted connection to concrete filled columns under cyclic loading: An experimental investigation. *Engineering Structures,* 46, 535-546.

WANG, J.-F., HAN, L.-H. & UY, B. 2009. Behaviour of flush end plate joints to concrete-filled steel tubular columns. *Journal of Constructional Steel Research,* 65, 925-939.

WANG, P., SUN, L., LIU, M., ZHANG, B., HU, X. & YU, J. 2020. Experimental studies on thread-fixed one-side bolted connection of beam to hollow square steel tube under static bending moment. *Engineering Structures,* 214**,** 110655.

WANG, P., SUN, L., XIA, C., GU, H., LIU, Y., LIU, M. & LIU, F. 2021a. Cyclic behavior of T-stub connection to hollow section steel column using TSOBs. *Journal of Constructional Steel Research,* 185**,** 106874.

WANG, P., SUN, L., ZHANG, B., YANG, X., LIU, F. & HAN, Z. 2021b. Experimental studies on T-stub to hollow section column connection bolted by T-head square-neck one-side bolts under tension. *Journal of Constructional Steel Research,* 178**,** 106493.

WANG, W., LI, M., CHEN, Y. & JIAN, X. 2017. Cyclic behavior of endplate connections to tubular columns with novel slip-critical blind bolts. *Engineering Structures,* 148**,** 949-962.

XUE, W., DING, M., WANG, H. & LUO, Z. 2008. Static Behavior and Theoretical Model of Stud Shear Connectors. *Journal of Bridge Engineering,* 13**,** 623-634.

YAO, H., GOLDSWORTHY, H. & GAD, E. 2008. Experimental and Numerical Investigation of the Tensile Behavior of Blind-Bolted T-Stub Connections to Concrete-Filled Circular Columns. *Journal of Structural Engineering,* 134**,** 198-208.

YU, Z., HOU, C., PENG, J. & HAN, L.-H. 2023. Experimental study on demountable CFST K-joints designed with blind bolts. *Thin-Walled Structures,* 187**,** 110723.

ZHU, J.-Y. & CHAN, T.-M. 2018a. Behaviour of polygonal-shaped steel-tube columns filled with high-strength concrete. *Proceedings of the Institution of Civil Engineers - Structures and Buildings,* 171**,** 96-112.

ZHU, J. & CHAN, T. 2018b. Experimental investigation on octagonal concrete filled steel stub columns under uniaxial compression. *Journal of Constructional Steel Research*, 147**,** 457-467.

List of Figures:

Table 1: Geometric dimensions of the tested specimens.

Specimen ID	Tube length (l) (mm)	Column section $(B \times B \times t_s)$ (mm)	B/t_s	Average bolt hole diameter, d_{hole} (mm)	Arrangement of hollo-bolts
B-E65-C40-T6.3	650	250×249×6.3	39.7	34.8	
B-E92-C40-T6.3	650	249×249.5×6.26	39.7	34.8	Two bolts in
B-E92-C40-T6.3-R	650	250×250×6.28	39.7	34.8	one-row
B-E107-C40-T6.3	650	250×249×6.28	39.7	35.0	
B-E107-C40-T6.3-P1	650	250×249×6.3	39.7	34.8	
C-E65-C40-T6.3	650	250×250×6.3	39.7	35.0	Two bolts in
C-E92-C40-T6.3	650	249×249.5×6.3	39.7	34.8	two-rows
C-E107-C40-T6.3	650	249×249.5×6.3	39.7	34.8	
D-E65-C40-T6.3	650	249×251×6.28	39.7	35.0	
D-E92-C40-T6.3	650	251×251×6.28	39.7	34.8	Four bolts in
D-E92-C40-T6.3-R	650	251×251×6.3	39.7	34.8	two-rows
D-E107-C40-T6.3	650	251×251×6.3	39.7	35.0	
D-E107-C40-T6.3-P1	650	251×251×6.3	39.7	35.0	

Table 2: Bolt geometric dimensions and other information of specimens.

Specimen ID	Average Bolt diameter, d_b (mm)	Nominal shear area of shank (A_t) (mm^2)	Net sleeve area (A_{sl}) (mm^2)	Bolt embedment length (mm)	Bolt torque (Nm)	Bolt Property class	Concrete cylinder character istic strength (MPa)
B-E65-C40-T6.3	20.0	245	431.9	65	300	8.8	40
B-E92-C40-T6.3	19.8	245	431.9	92	300	8.8	40
B-E92-C40-T6.3-R	19.7	245	431.9	92	300	8.8	40
B-E107-C40-T6.3	20.1	245	431.9	107	300	8.8	40
B-E107-C40-T6.3-P1	19.7	245	431.9	107	300	8.8	40
C-E65-C40-T6.3	19.8	245	431.9	65	300	8.8	40
C-E92-C40-T6.3	19.8	245	431.9	92	300	8.8	40
C-E107-C40-T6.3	20.0	245	431.9	107	300	8.8	40
D-E65-C40-T6.3	19.8	245	431.9	65	300	8.8	40
D-E92-C40-T6.3	19.7	245	431.9	92	300	8.8	40
D-E92-C40-T6.3-R	19.8	245	431.9	92	300	8.8	40
D-E107-C40-T6.3	19.8	245	431.9	107	300	8.8	40
D-E107-C40-T6.3-P1	19.8	245	431.9	107	300	8.8	40

Table 3: Material properties of steel tubes and blind-bolts. (Debnath and Chan, 2022b)

Steel Material		Yield strength, (f_y) (MPa)	Ultimate strength, (f_u) MPa)	Elastic Modulus, (E_s) (GPa)	f_u/ f_y
Steel tube	250 × 250 × 6.3 mm	373.0	491.3	194.4	1.31
M20 diameter blind-bolt	Shank length 120 mm	793.6	934.5	208.4	1.17
	Shank length 150 mm	839.0	967.7	205.9	1.15
	Shank length 165 mm	799.1	887.7	208.6	1.11
	Sleeve*	393.0	523.0	_	1.33

Note: * average sleeve material properties based on hardness test.

Table 4: Test results of specimens under shear forces.

Specimen ID	S_u (mm)	S_{max} (mm)	$F_{v,max}$ (kN)	k (kN/mm)	k_{sc} (kN/mm)	Failure mode
B-E65-C40-T6.3	9.05	10.16	462	94.34	77.36	Sleeve and shank failure
B-E92-C40-T6.3	8.35	9.45	510.5	99.02	84.28	Sleeve and shank failure
B-E92-C40-T6.3-R	8.68	10.5	544	76.40	79.33	Sleeve and shank failure
B-E107-C40-T6.3	8.35	9.7	528	130	87.81	Sleeve and shank failure
B-E107-C40-T6.3-P1	10.1	11.52	565	66.67	66.63	Sleeve and shank failure
C-E65-C40-T6.3	9.30	10.70	490	115.6	77.86	Sleeve and shank failure
C-E92-C40-T6.3	8.35	9.55	500.5	92.8	78.3	Sleeve and shank failure
C-E107-C40-T6.3	7.22	9.40	498.5	160.1	92.54	Sleeve and shank failure
D-E65-C40-T6.3	9.8	11.17	1052	136.7	150.9	Sleeve and shank failure
D-E92-C40-T6.3	10.5	12.7	1060.5	142	127.3	Sleeve and shank failure
D-E92-C40-T6.3-R	9.10	10.5	1056	180	152.3	Sleeve and shank failure
D-E107-C40-T6.3	7.95	8.25	960	208.3	173	Sleeve and shank failure
D-E107-C40-T6.3-P1	9.05	9.275	1032.5	201.7	163.5	Sleeve and shank failure

Table 5: Summary of joint shear strength analysis.

Specimen ID	Measured $F_{\mathrm{v,max}}$ (kN)	Measured $F_{\mathrm{v}}/F_{\mathrm{v,max}}$	(Measured $F_{\mathrm{v}}/F_{\mathrm{v,max}}$)/ (Calculated $F_{\mathrm{v}}/F_{\mathrm{v,max}}$)	Measured $F_{\mathrm{v}}/F_{\mathrm{v,max}}$	(Measured $F_{\mathrm{v}}/F_{\mathrm{v,max}}$)/ (Calculated $F_{\mathrm{v}}/F_{\mathrm{v,max}}$)	Calculated shear strength of group hollo-bolted CFST joint ($n \times F_{\mathrm{v,max}}$) (kN)	(Measured $F_{\mathrm{v,max}}$) / (Calculated $F_{\mathrm{v,max}}$)
B-E65-C40-T6.3	462	0.5	0.71	1.0	1.13	503	0.91
B-E92-C40-T6.3	510.5	0.5	0.73	1.0	1.04	507	1.00
B-E92-C40-T6.3-R	544	0.5	0.90	1.0	1.08	485	1.12
B-E107-C40-T6.3	528	0.5	0.74	1.0	1.04	485	1.08
B-E107-C40-T6.3-P1	565	0.5	1.17	1.0	1.26	485	1.16
C-E65-C40-T6.3	490	0.5	0.81	1.0	1.16	503	0.97
C-E92-C40-T6.3	500.5	0.5	0.87	1.0	1.04	507	0.98
C-E107-C40-T6.3	498.5	0.5	0.70	1.0	0.90	485	1.02
D-E65-C40-T6.3	1052	0.5	0.98	1.0	1.22	1006	1.04
D-E92-C40-T6.3	1060.5	0.5	1.12	1.0	1.31	1015	1.04
D-E92-C40-T6.3-R	1056	0.5	0.93	1.0	1.13	1015	1.04
D-E107-C40-T6.3	960	0.5	0.70	1.0	0.99	970	0.98
D-E107-C40-T6.3-P1	1032.5	0.5	0.82	1.0	1.13	970	1.06
Mean			*0.86*		*1.13*		*1.03*
CoV			*0.02*		*0.01*		*0.004*

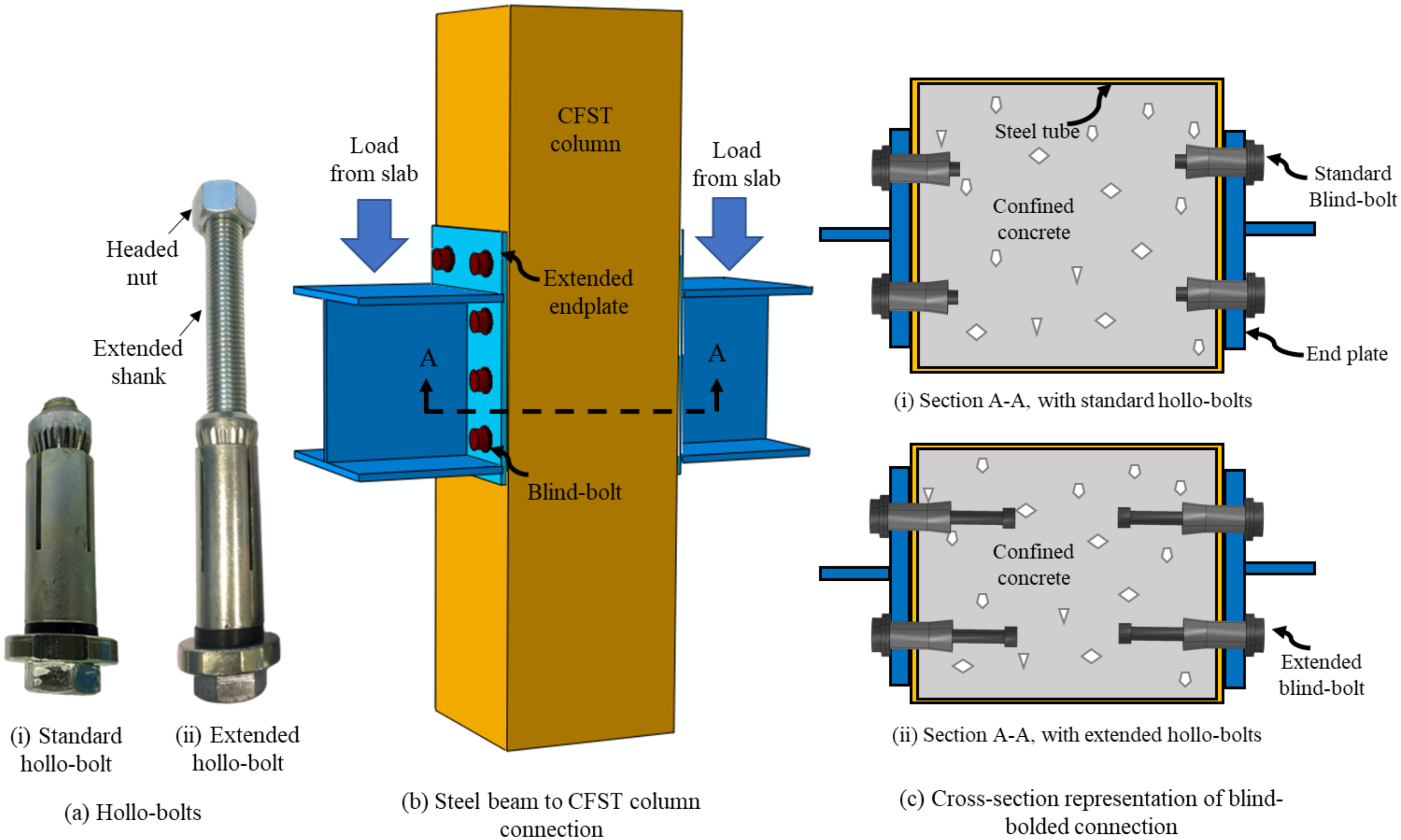

Figure 1: (a) Hollo-bolts, (b) hollo-bolted beam-column joint (c) cross-section of the joint.

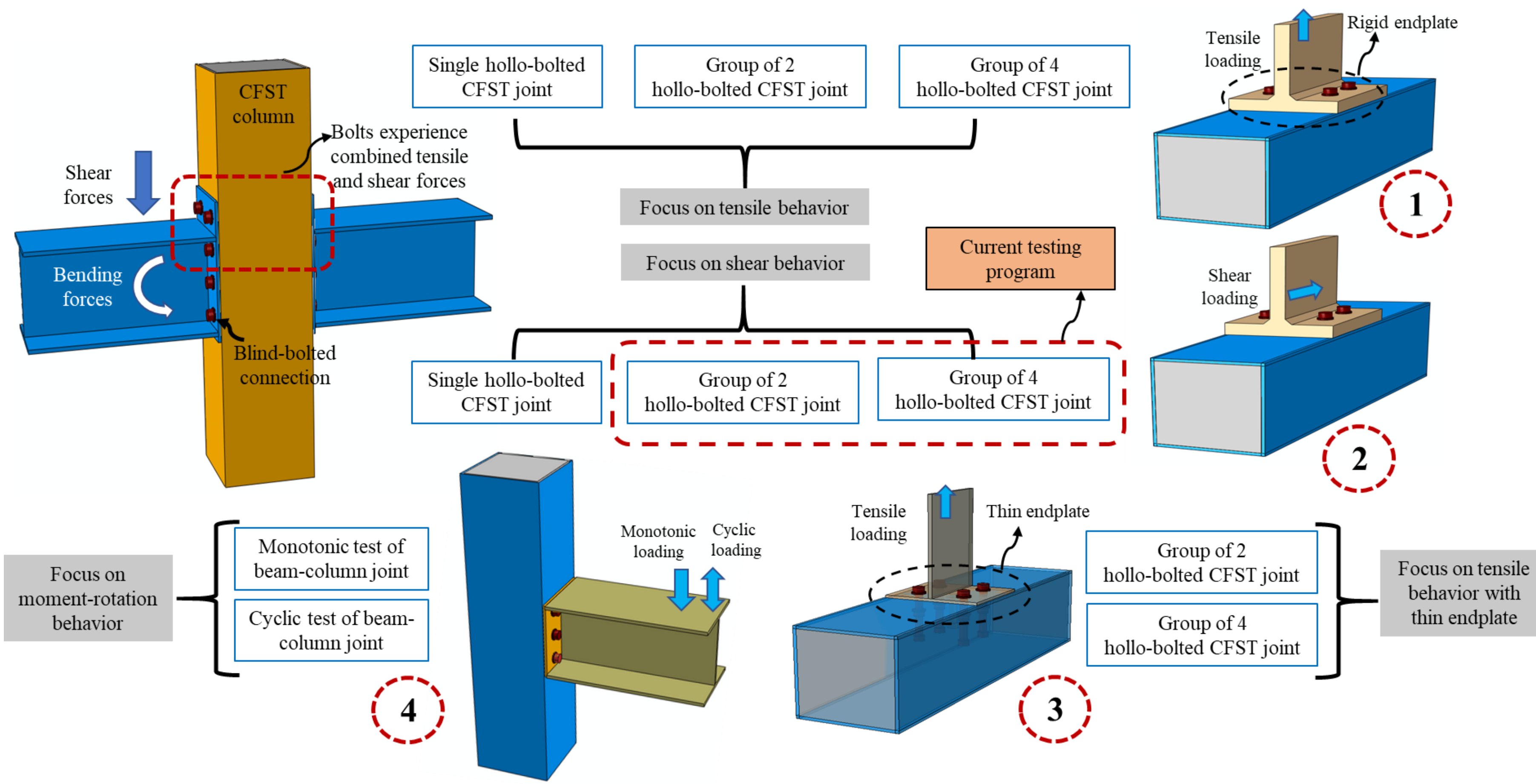

Figure 2: Framework for the development of hollo-bolted CFST moment joints.

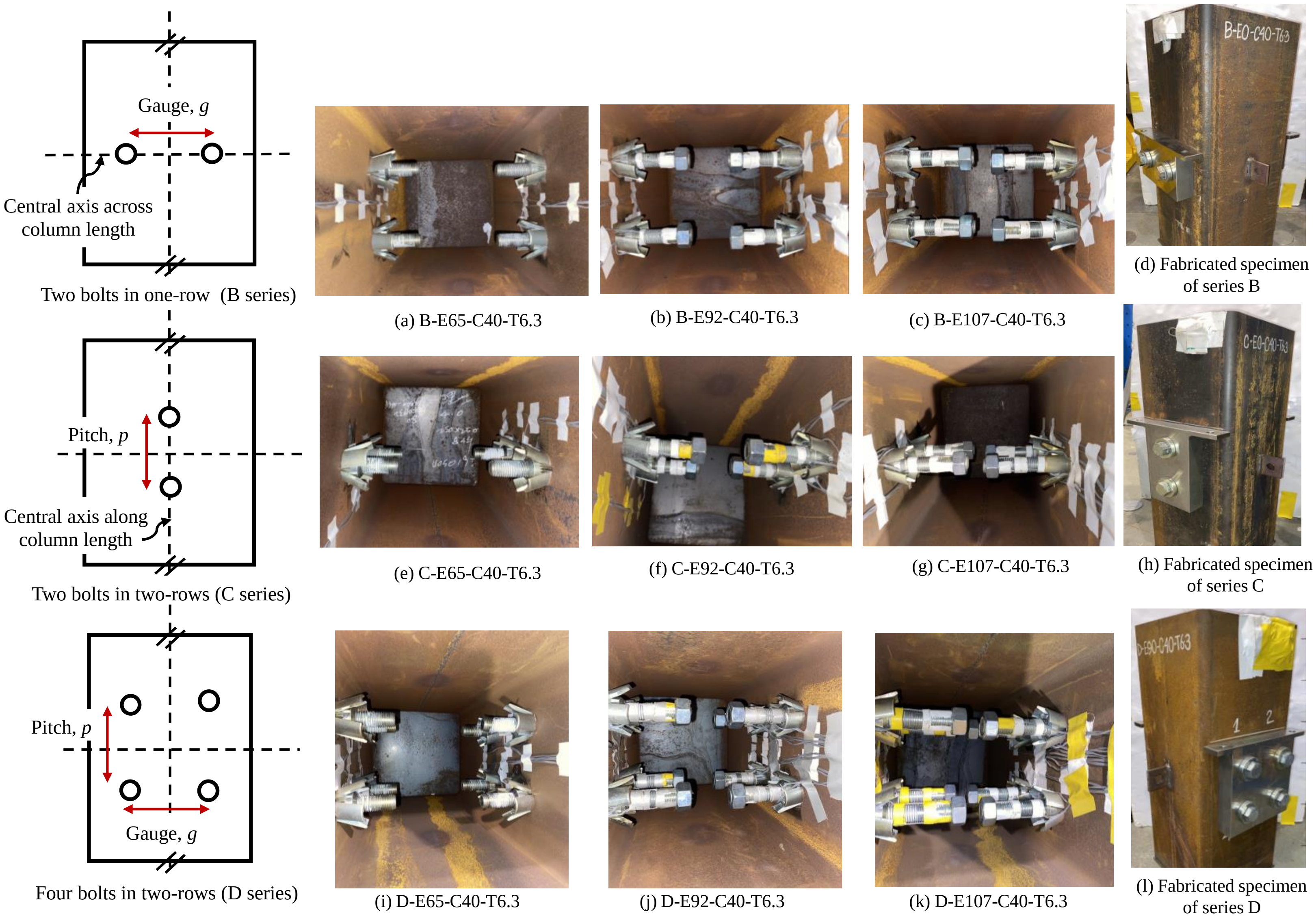

Figure 3: Specimens in series B, series C and series D.

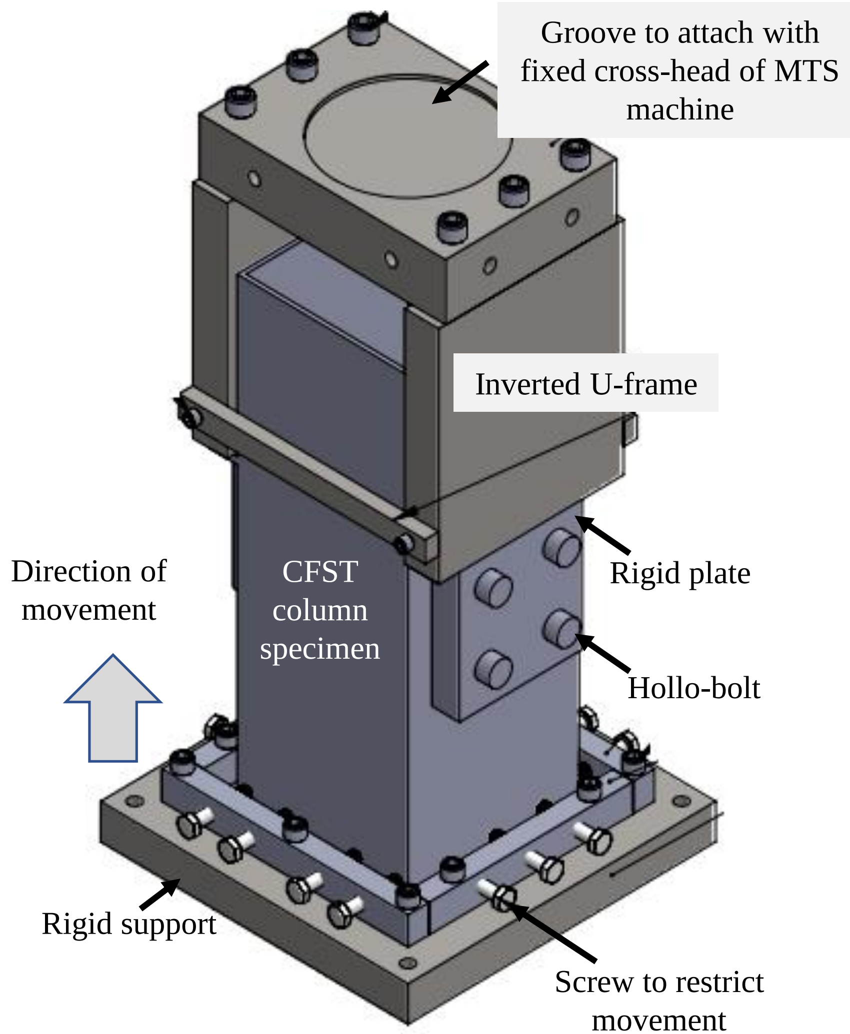

Figure 4: 3D diagram for laboratory test setup.

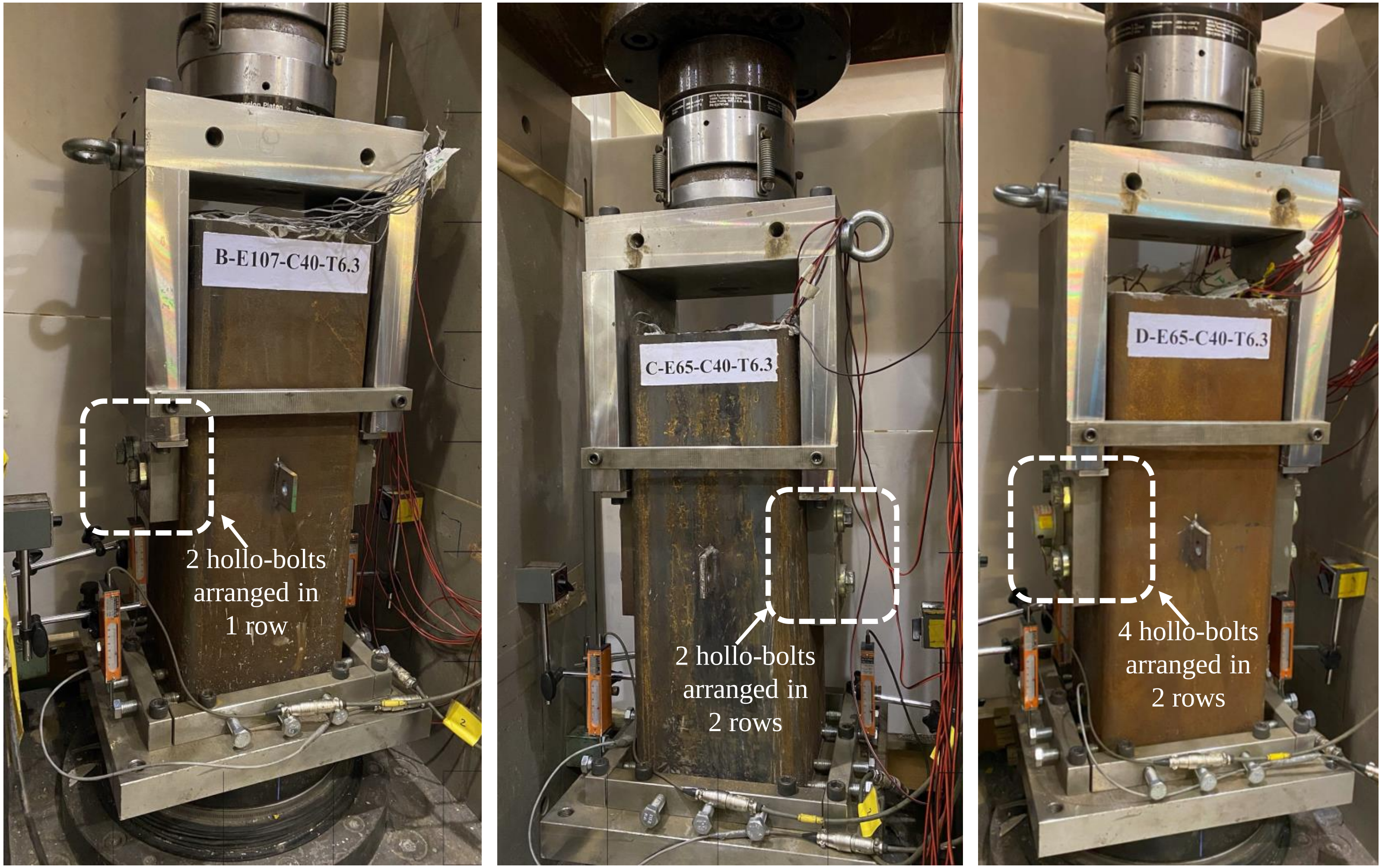

(a) Series B specimen   (b) Series C specimen   (c) Series D specimen

Figure 5: Experimental test setup in MTS rock mechanic machine.

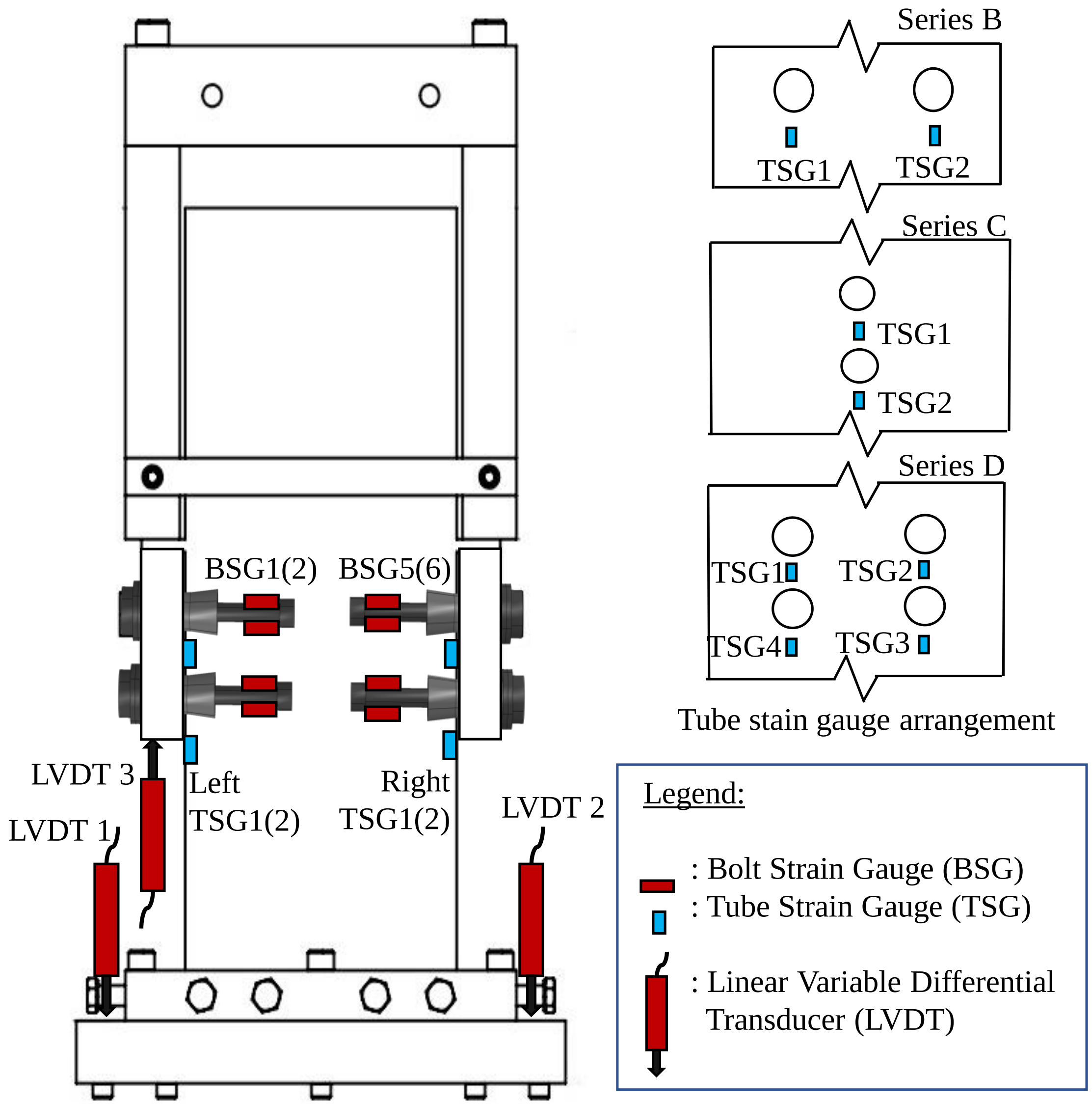

Figure 6: Instrumentation used in the experiment.

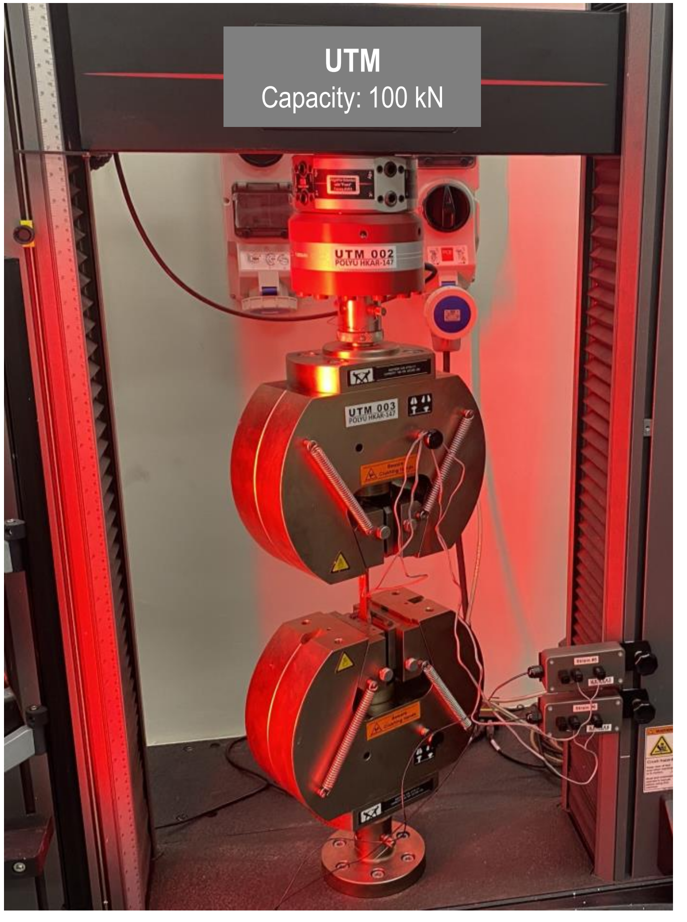
UTM
Capacity: 100 kN
UTM 002
POLYU HKAR-147
UTM 003
POLYU HKAR-147

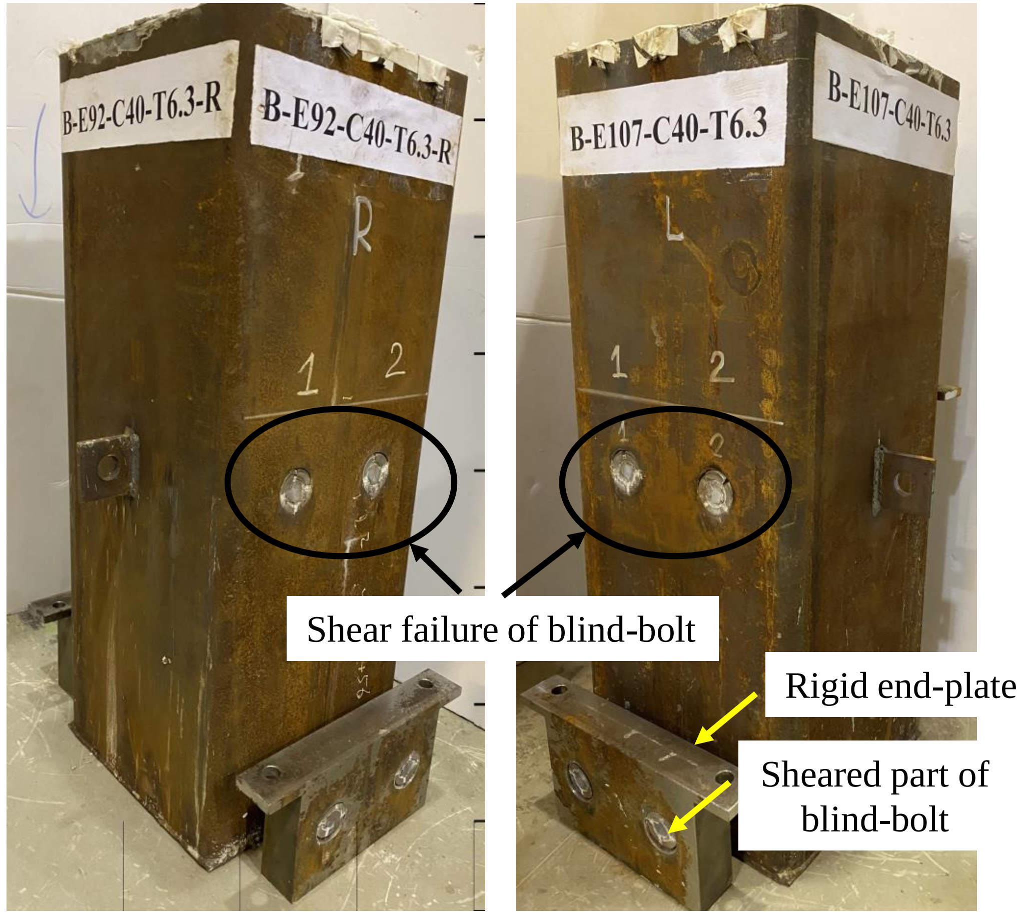

(a) Specimen: B-E92-C40-T6.3-R (b) Specimen: B-E107-C40-T6.3

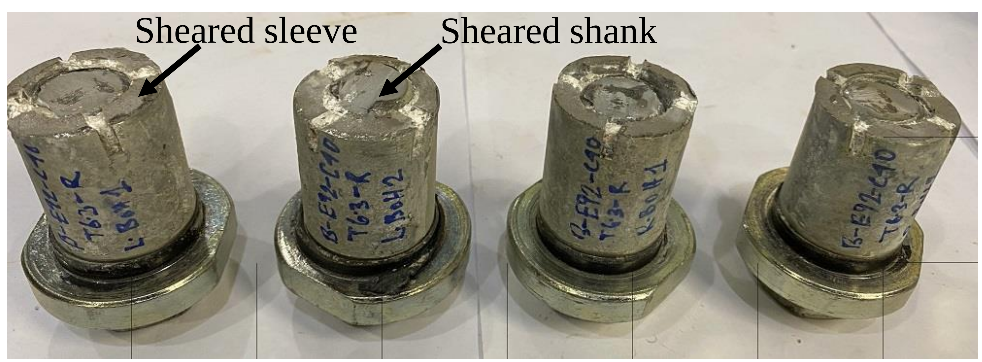

(c) Blind-bolts after failure in specimen B-E92-C40-T6.3-R

Figure 8: Failure of specimens in Series B after testing.

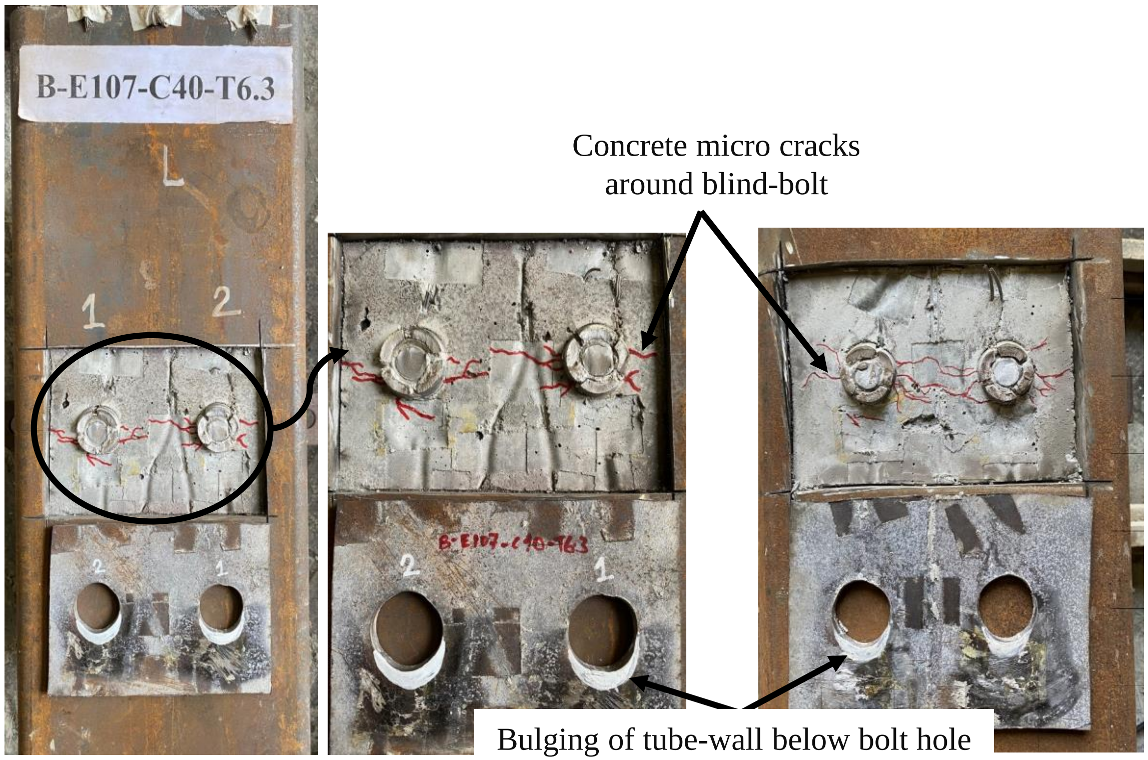

(a) Specimen: B-E107-C40-T6.3 (b) Specimen: B-E107-C40-T6.3-P1

Figure 9: Concrete and inner surface of tube-wall after test.

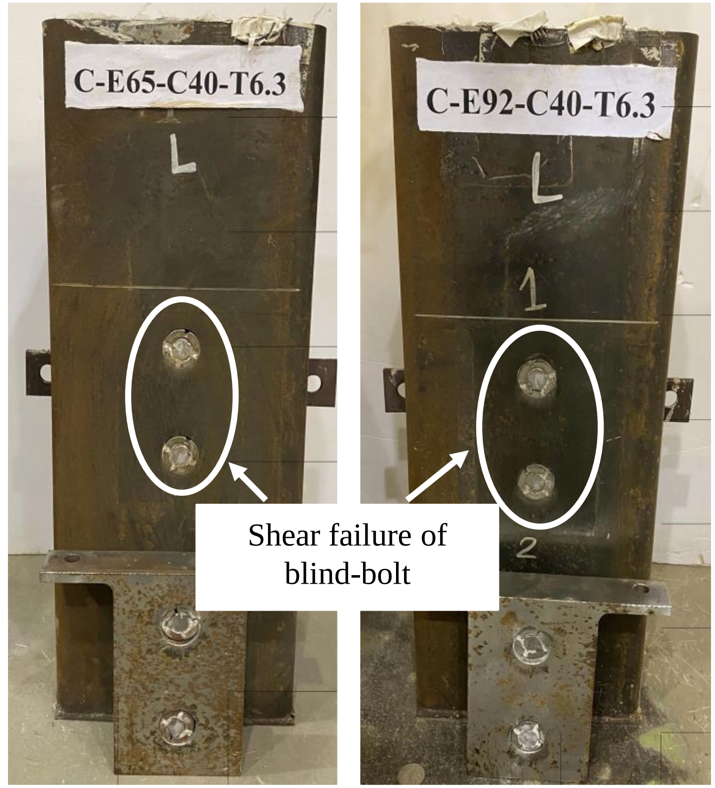

Figure 10: Specimens in series C after testing.

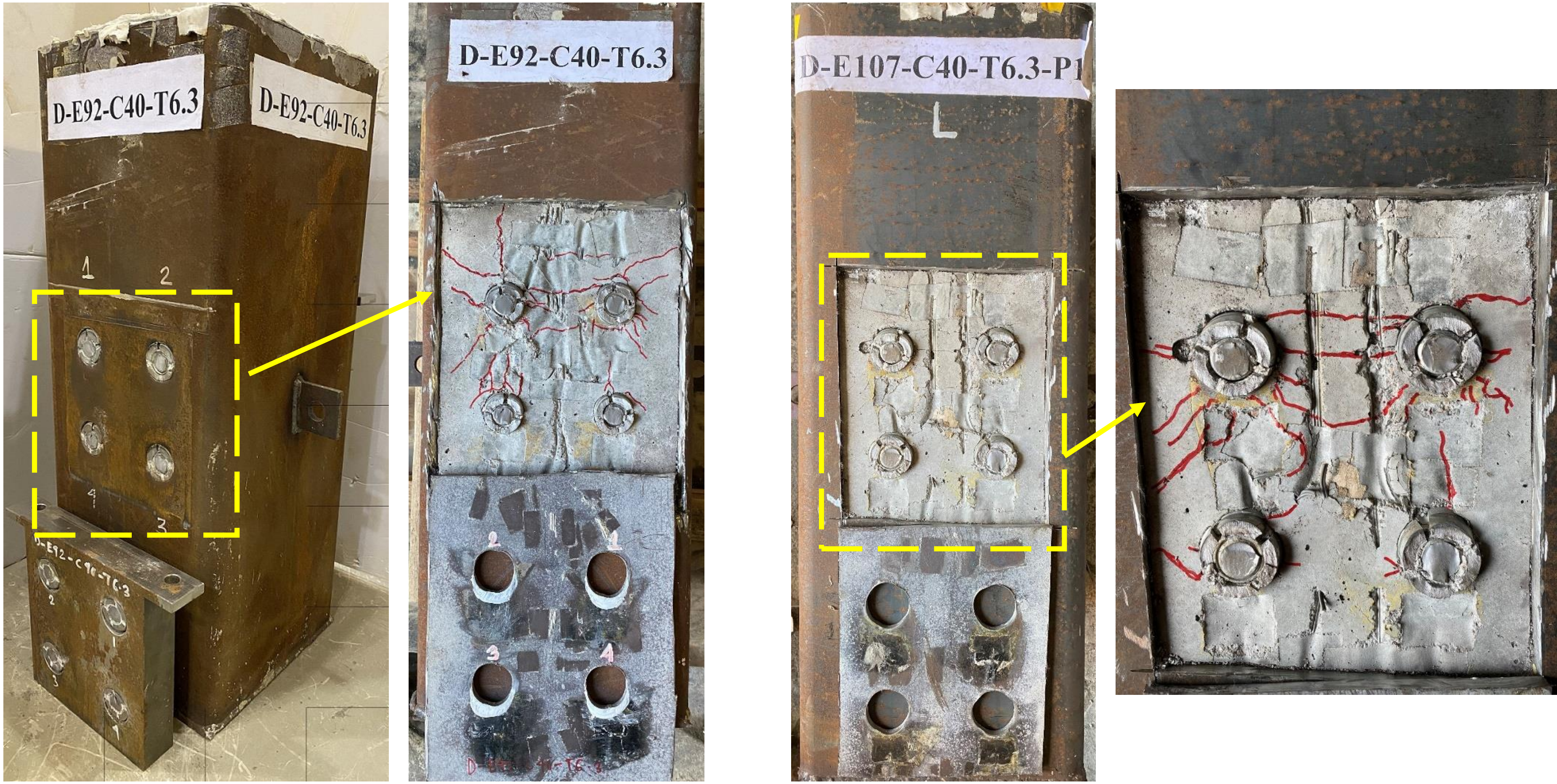

(a) D-E92-C40-T6.3

(b) D-E107-C40-T6.3-P1

Figure 11: Specimens in series D after testing.

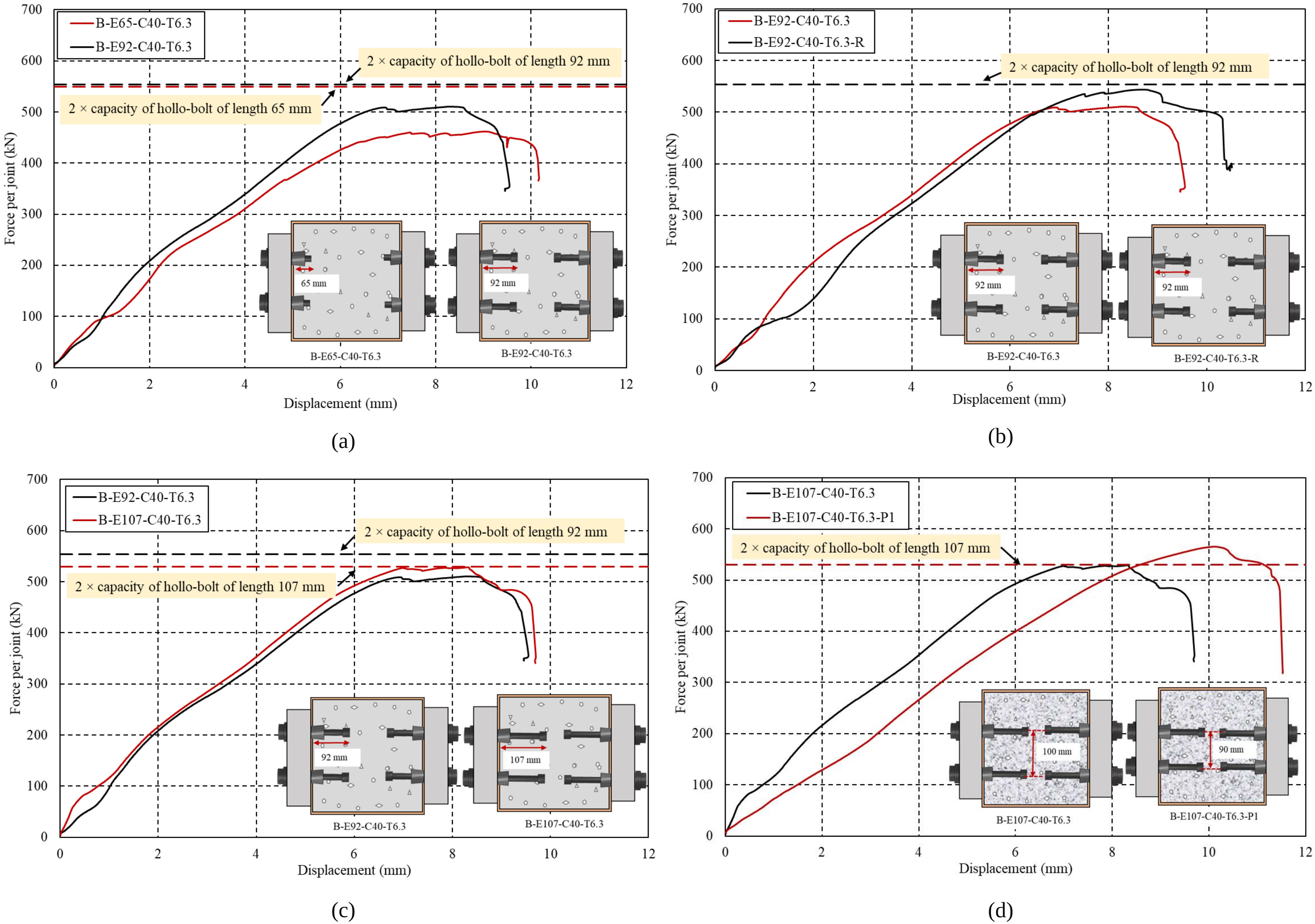

Figure 12: Load-displacement behavior of specimens of Series B.

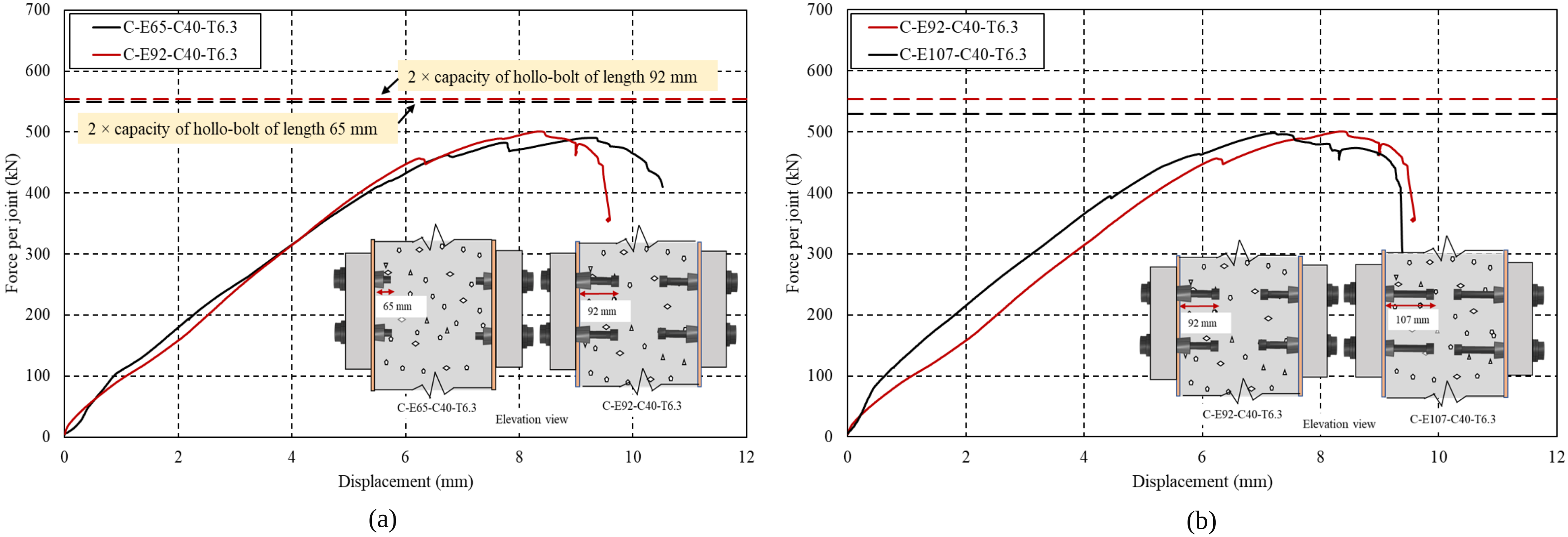

Figure 13: Load-displacement behavior of specimens of Series C.

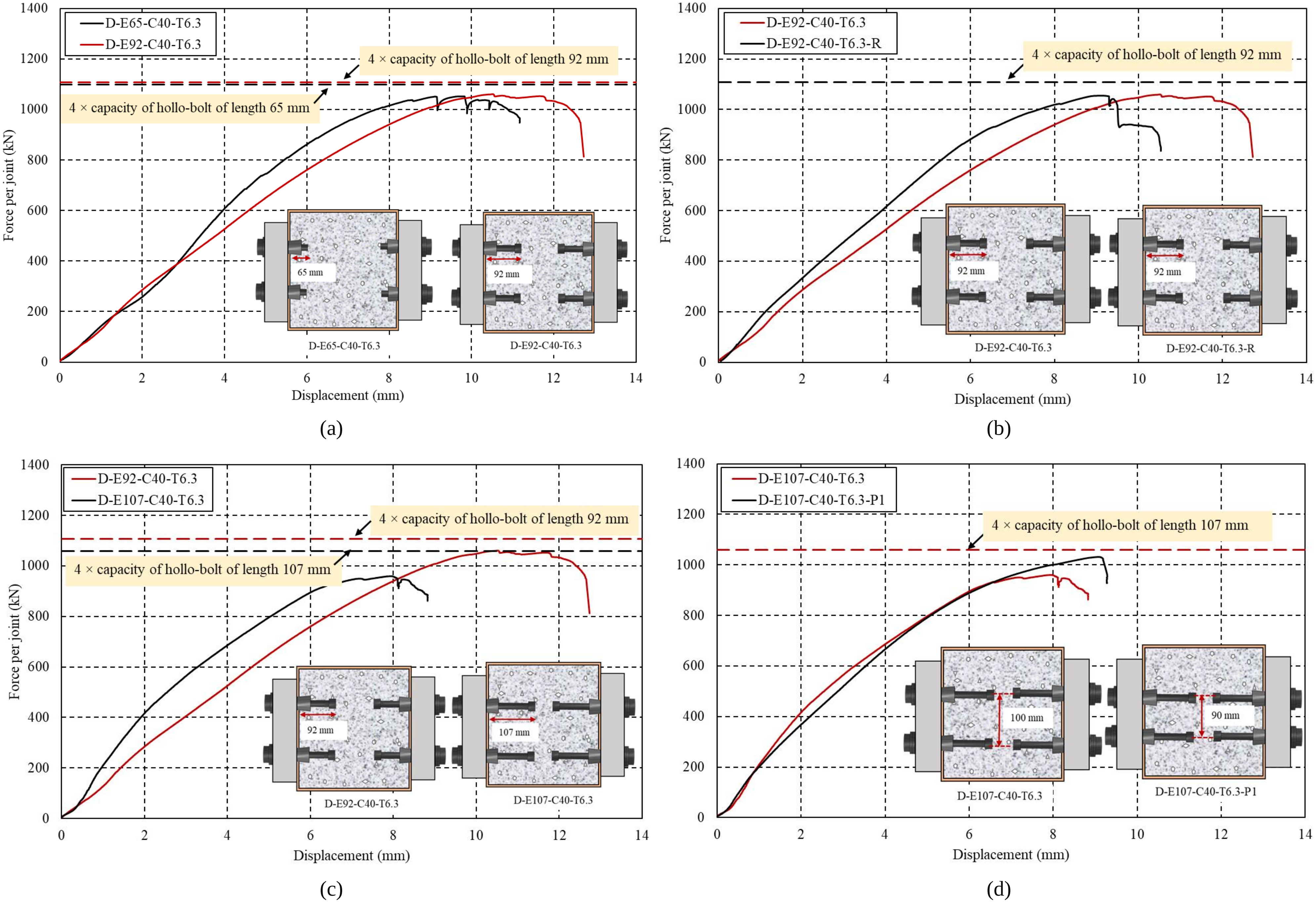

Figure 14: Load-displacement behavior of specimens of Series D.

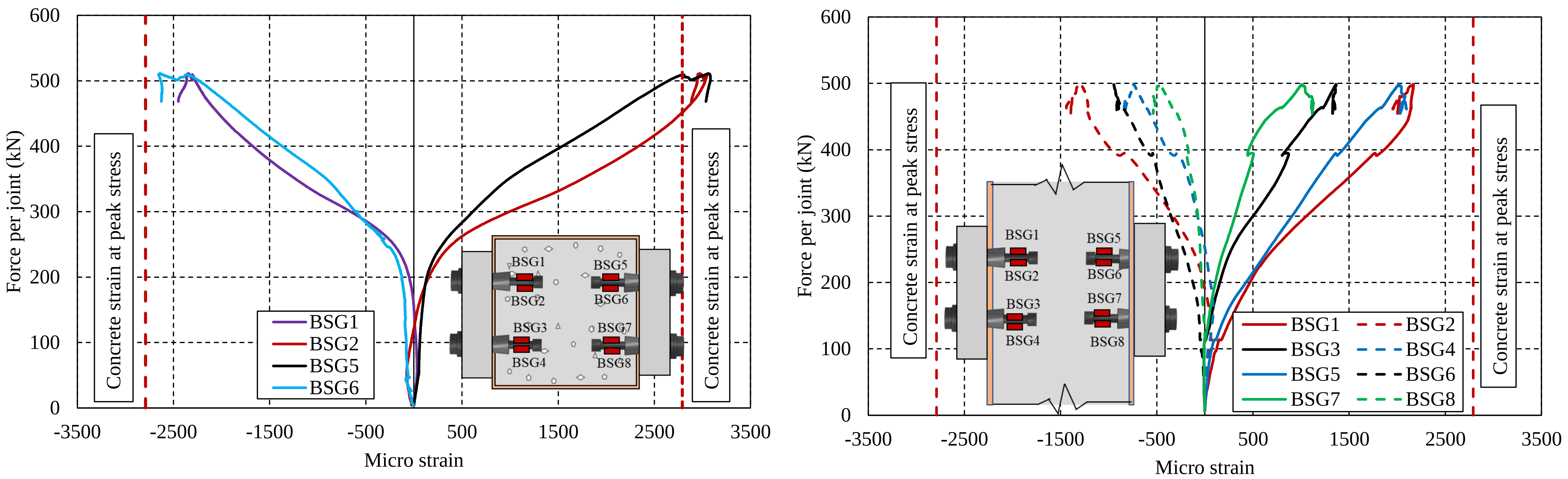

(a) B-E92-C40-T6.3

(b) C-E107-C40-T6.3

Figure 15: Development of strain in anchored hollo-bolt shank.

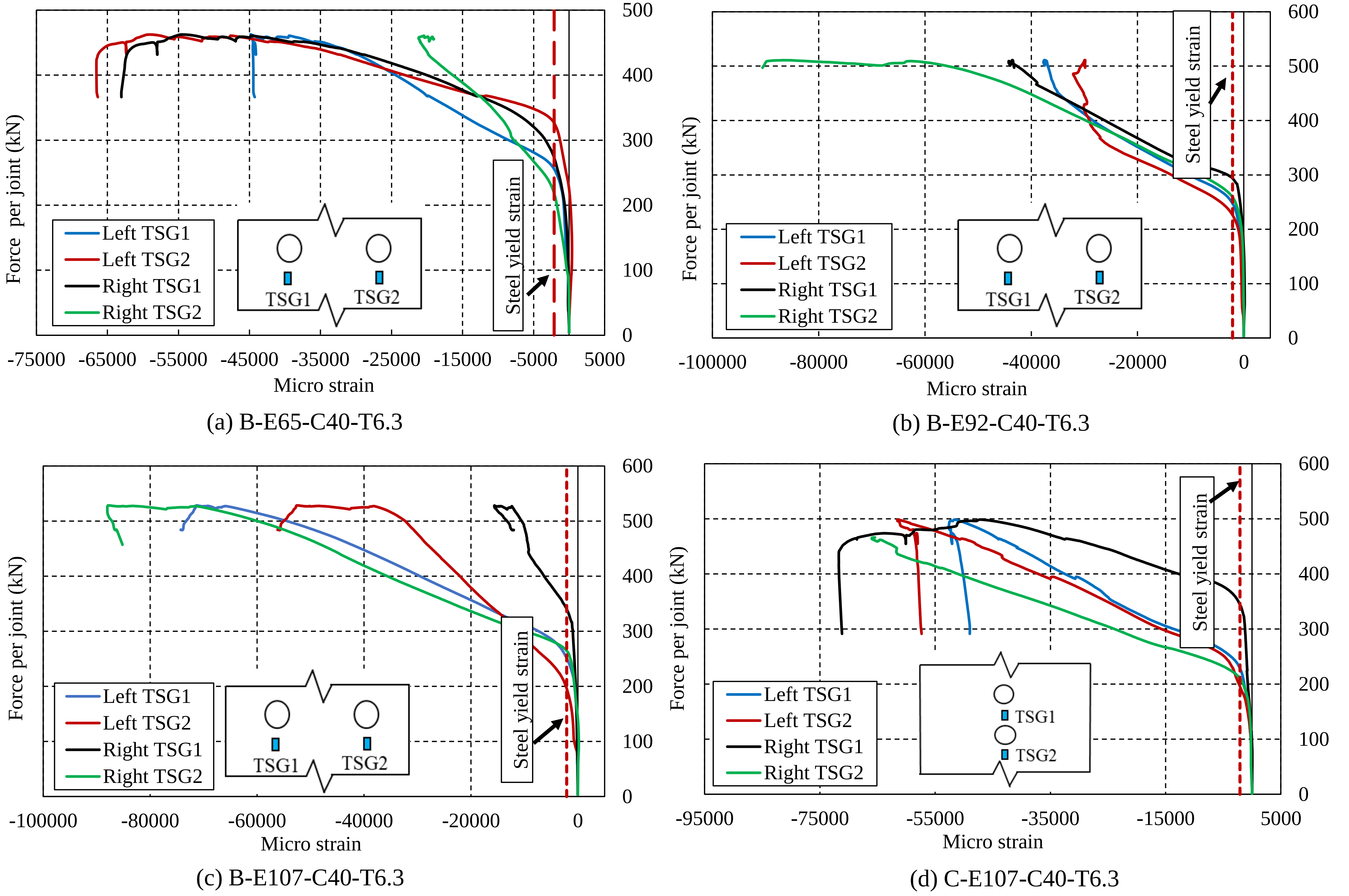

Figure 16: Representative plots of local strain developed in steel tube of CFST specimens.

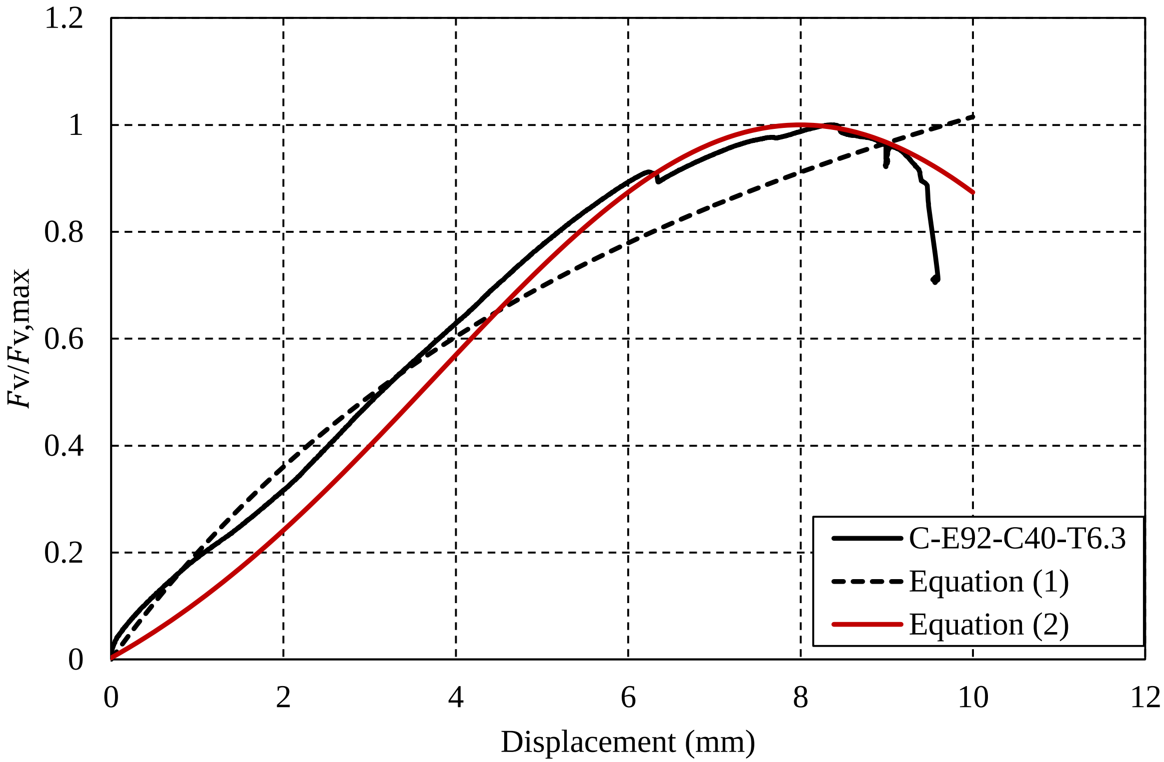

Figure 17: Comparison of sample test result and regression curves.

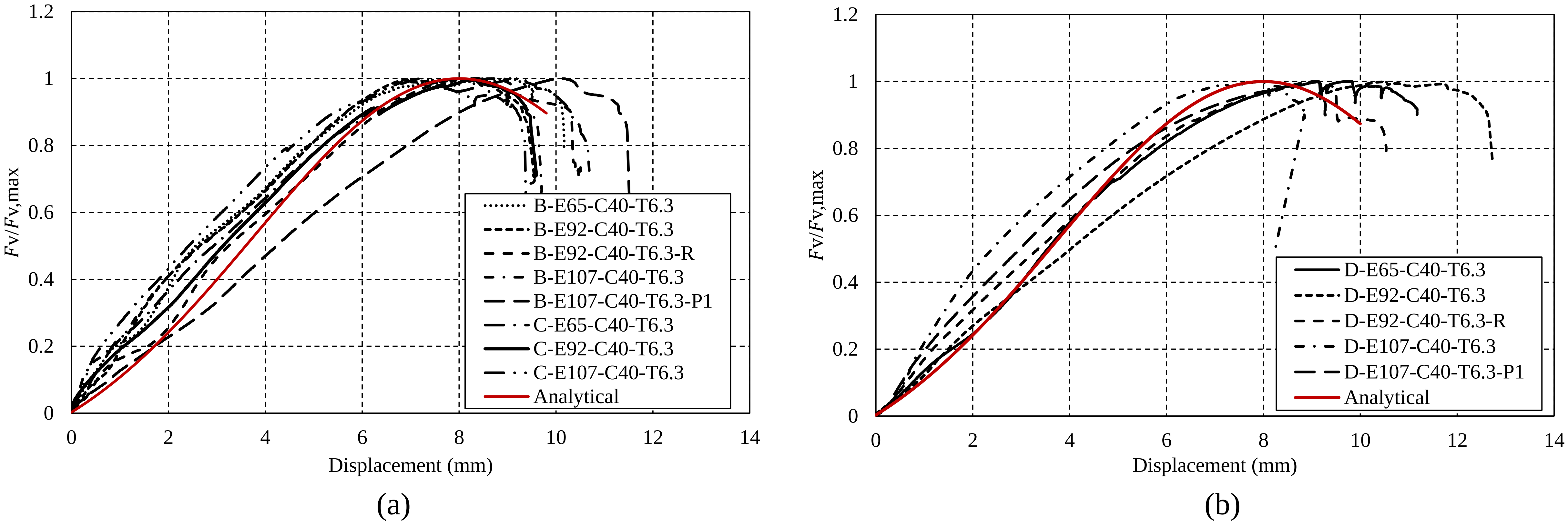

Figure 18: Comparison of analytical and experimental force-displacement curves for (a) series B and C; (b) series D.